Chapter 8
Forward and Inverse Solutions for Two-Element Risley-Prism-Based Beam-Steering Systems in Different Configurations

There are two basic problems regarding applications of Risley-prism-based beam-steering systems for directing a laser beam to illuminate a point of interest. First, given the two prisms' orientations, in what direction does the laser beam propagate after emerging from the system? The second problem may be regarded as the inverse of the first one, i.e., given the required pointing position, what will be the orientations of the prisms? The answer to the first problem can be found in a number of publications [7.9, 7.18, 7.19, 7.25] as summarized in Chapter 7. Investigations of the second problem, which is known as the inverse problem or the problem of precise pointing [7.9, 8.1–8.4], have been stimulated by the applications of Risley prism pairs to optical tracking and pointing at targets in free space.

Solutions for the inverse problem, which can be regarded as exact, are very rare in the literature. Historically, Amirault and DiMarzio found in their 1985 paper [8.1] some difficulties in inverting the vector equations for refraction at the surfaces of the prisms for an exact solution to the problem of precise pointing using Risley prism pairs. However, they proposed a realistic approach to obtain an inverse solution through a two-step method, which will be specified in this chapter. Ten years later, Boisset and Robertson et al. [8.2] proposed a paraxial method and developed an iterative algorithm to solve the inverse problem. Furthermore, Degnan [8.3] developed in 2002 a first-order approximation method that does not need an iterative algorithm to find prisms' orientations for a given pointing position. Recently, Li proposed a third-order solution for the inverse problem [7.9]. The first exact solution was given in 2008 by Yang [8.4], who investigated the case of a Risley prism pair having two identical dispersive prisms, i.e., prisms whose principal cross

Table 8.1 Dependence of the maximum extent of beam steering angle on the ray deviation power of Risley prism pair. Comparison of the predictions of third-order theory and solution from Eq. (8.11a) about the prism angle α for refractive index $n = 1.5$ and 4.0.

The required altitude angle $\Phi =$		10°	20°	30°	40°
$n = 1.5$	Third-order prediction $\alpha \geq$	9.99°	19.90°	29.69°	39.19°
	Equation (8.11a) for $\alpha \geq$	9.76°	18.16°	24.41°	28.41°
	Percentage difference	2.3(%)	9.2(%)	17.8(%)	27.5(%)
$n = 4.0$	Third-order prediction $\alpha \geq$	1.67°	3.32°	4.94°	6.53°
	Equation (8.11a) for $\alpha \geq$	1.65°	3.24°	4.67°	5.91°
	Percentage difference	1.2(%)	2.4(%)	5.5(%)	9.5(%)

sections are isosceles triangles, whereas this chapter presents the exact inverse solutions for systems that contain two thin wedge prisms because the thin wedges are ideal for laser beam steering and are now commonly used in real devices.

This chapter applies the analytic results developed in Chapter 7 to formulate the inverse solution for laser beam pointing with Risley-prism-based beam-steering systems. Both exact and approximate solutions are found and the accuracy of their predictions is compared numerically through case studies relating to systems working with visible and infrared wavelengths. The exact solution of the inverse problem is generalized from pointing at a single point target to steering a laser beam to highlight a specific pattern.

The main references of this chapter are Refs. [7.9] and [8.8].

8.1 First-Order Graphical and Analytical Solutions for Target Tracking

First- and third-order approximations to the inverse solution of the Risley prism pointer may not provide adequate accuracy for precise pointing a laser beam at a remote target. We are still interesting in these approximations because of a better understanding of the significance of the parameters, variables, and formulation of the theory of precise pointing. Secondly, predictions of approximate and exact theories are very close [see Table 8.2 below], and we may use the easily obtainable approximate results as the starting condition for iterative approach to a required solution. Finally, taking advantage of the straight-forward graphic results from the approximate theories to reduce uncertainty in computations of multivalued functions, such as the choice of plus or minus sign in front of the square root and to avoid the ambiguity in evaluation of inverse trigonometric functions.

The key parameters in the first- and third-order approximations are δ_1 and δ_2, [see Eq. (7.1)], i.e., the power of ray deviation between the incident and emerging rays of the thin prisms in Risley prism pair. The variables in the

Table 8.2 Comparison of the computed results obtained from different theories for Risley prism pointer of the A-1 configuration in the Group A. Two identical prisms of index $n = 4.0$ and prism angle $\alpha = 5°$ are used for pointing the target at altitude $\Phi = 4.5°$ and azimuth $\Theta = 120°$.

Angular Parameters	$(\Delta\theta)_0$	ψ_0	θ_1	θ_2
First-Order Approximation	162.746°	81.373°	38.627°	201.373°
Third-Order Approximation	162.751°	81.569°	38.431°	201.182°
Exact Solution	162.768°	81.578°	38.422°	201.190°

first- and third-order approximations and also in the exact theory are the rotation prism angles θ_1 and θ_2, and their difference $\Delta\theta$, as defined in Eqs. (7.2).

8.1.1 Vector-based graphics of the first-order inverse solutions

The precise pointing of laser beam at a remote target is the problem of steering the laser beam to specific altitude (i.e., elevation or magnitude) angle Φ and the azimuth angle Θ within the angular range of the system [7.2, 7.3]. Here Φ is the angle of the beam relative to the z axis and Θ is the angle around the z axis, all counted from the xz-plane (see Fig. 8.1).

The two prisms shown in Fig. 8.1 are rotatable about the z-axis, their angular positions are specified by their respective rotation angles θ_1 and θ_2 counted from the xz-plane. The incident ray propagates in the direction specified by the ray direction vector $\hat{\mathbf{s}}_{11}^{(i)}$ and the ray is deviated by the first prism Π_1 by an angle, the power and direction are shown together by the vector $\boldsymbol{\delta}_1$, for the second prism Π_2 we have vector $\boldsymbol{\delta}_2$, both vectors are shown in Fig. 8.1. According to the first-order approximation [see, e.g., Sect. 2.4 in

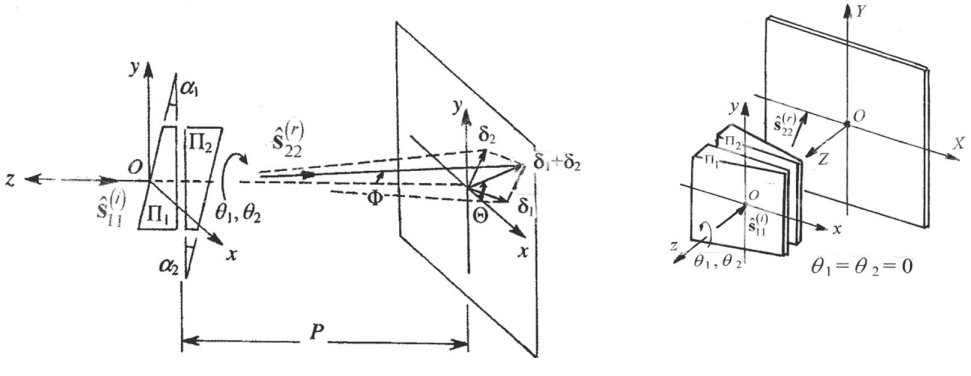

Figure 8.1 Illustrating notation and coordinates for Risley prisms Π_1 and Π_2 of indices n_1 and n_2, and prism angles α_1 and α_2. Unit vector $\hat{\mathbf{s}}_{11}^{(i)}$ of the incident ray in the direction collinear with the z-axis, i.e., the axis of prisms rotation. Prisms at rest position ($\theta_1 = \theta_2 = 0$) is shown on the right.

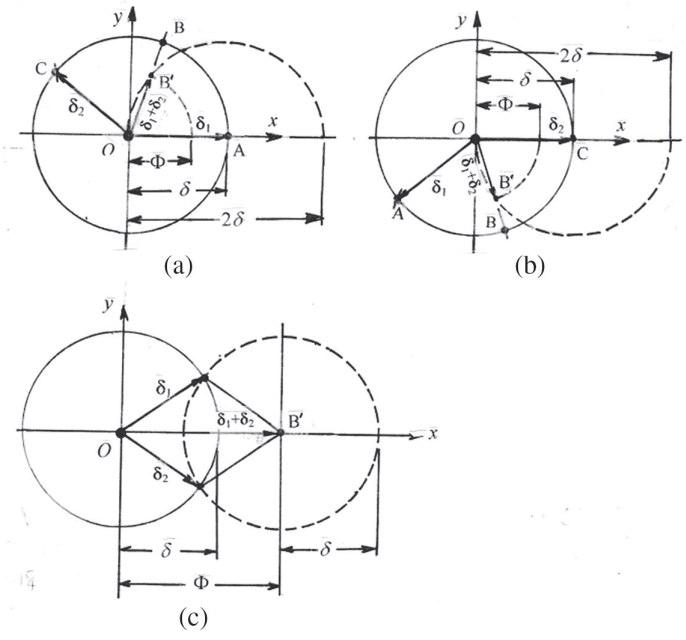

Figure 8.2 The graphic method of vector-based first-order approximation for determination of θ_1 and θ_2 of the two rotary prisms for steering optical beam into the direction specified by the altitude Φ and azimuth Θ. Assume $\delta_1 = \delta_2 = \delta = (n-1)\alpha$, i.e., a matched prism pair is used [see, e.g., Eq. (7.1)]. (a) Rotation of the second prism to meet the requirement of the altitude angle Φ and then rotation the two prisms together to meet the requirement of the altitude angle Θ. (b) Rotation of the first prism first and then rotation the two prisms together. (c) Rotation of the two prisms simultaneously first to meet the requirement of the altitude angle Φ and then rotation the two prisms together to meet the requirement of the altitude angle Θ.

Ref 8.1], the two deviations add vectorially on the plane of observation, as shown by the vector $\boldsymbol{\delta}_1 + \boldsymbol{\delta}_2$ in Fig. 8.1.

The next step shows a vector-based graphics about the two-step method [8.1] of steering laser beam to the direction specified by the altitude angle Φ and the azimuth angle Θ (see Fig. 8.1) based on the use of a compass, a ruler, and the classical geometric construction techniques.

- The first step is to keep the prism Π_1 at $\theta_1 = 0$ and rotating the second prism Π_2 to the angle $(\Delta\theta)_0$ [see, e.g., Eqs. (8.4) and (8.12) below]. After that, the orientations of the two prisms are given $\theta_1 = 0$ and $\theta_2 = (\Delta\theta)_0$ and the beam is directed to a point of altitude Φ and azimuthal angle ψ_0.
- The second step of this method is a co-rotation of the two prisms from the angle ψ_0 to the required azimuth Θ. The two-step method is shown in Figs. 8.2 and 8.3.

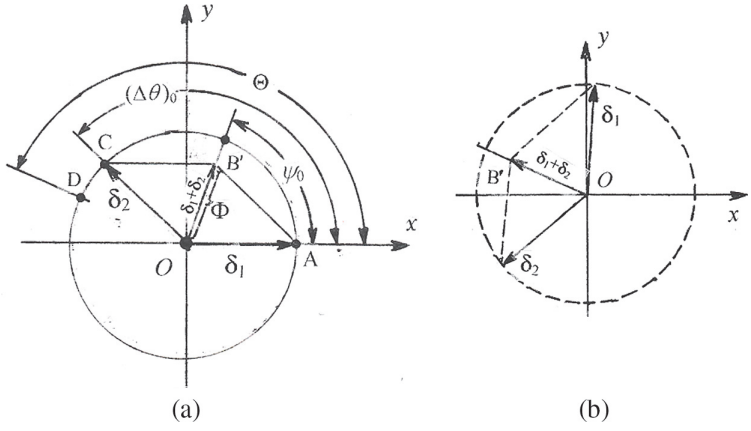

Figure 8.3 Graphical calculation of first-order solutions of the inverse problem relating to Risley prism pointer for poiting a laser beam to the direction specified by the altitude angle Φ and azimuth angle Θ. Assume two prisms with identical power of ray deviation: $\delta_1 = \delta_2 = \delta$. (a) Illustrating notation relating to rotation of the second prism an angle $(\Delta\theta)_1$ to meet the requirement of the altitude angle Φ and then (b) co-rotation the two prisms an angle $\Theta - \psi_0$ to meet the requirement of the altitude angle Θ.

Figure 8.2(a) shows the case when the second prism rotates first to meet the requirement of the altitude angle Φ and then rotating the two prisms together to meet the requirement of the azimuth angle Θ. The graphic calculation can be summarized as

- Centered at the origin of the rectangular coordinates system Oxy, draw a circle of radius δ in solid line; let the ray deviation vector $\boldsymbol{\delta}_1$ of the first prism at rest in the position parallel and coincided with the x axis, as shown by the vector $\overrightarrow{OA}$ in Fig. 8.2(a).
- Centered at the point ($x = \delta$, $y = 0$), draw an auxiliary half circle of radius δ in dashed line above the x axis.
- Centered at the origin, draw another auxiliary circle of radius Φ above the x axis that intersects the dashed line half circle at the point B′ (see Fig. A9 in Section A3 of the Appendix A). Extend the line segment $\overline{OB'}$ until meeting the solid line circle of radius δ at the point B, that is the mid-point of the angle $(\Delta\theta)_0$ between the two ray deviation vectors $\boldsymbol{\delta}_1$ and $\boldsymbol{\delta}_2$. Here the length of the radius Φ is (Φ/δ) unit of the length of δ.
- Using the point B as the pivot point of the needle of your compass to draw a circle of radius $\overline{BA}$, that intersects the circle of radius δ in solid line at the point C and the vector $\overrightarrow{OC} = \boldsymbol{\delta}_2$.
- Co-rotating the two prisms until $\boldsymbol{\delta}_1+\boldsymbol{\delta}_2$ to meet the requirement of the azimuth angle Θ [see, e.g., Fig. 9.5(d)].

Similar geometric construction is shown in Fig. 8.2(b) about the two-step method applied to the case of rotating the first prism first to meet the requirement of the altitude angle Φ and then rotating the two prisms together to meet the requirement of the azimuth angle Θ.

Slightly different geometric construction is shown in Fig. 8.2(c) about the two-step method for the case of rotating the two prisms simultaneously to meet the requirement of the altitude angle Φ and then rotating the two prisms together to meet the requirement of the azimuth angle Θ. It is seen that the half circles in the dashed lines in Figs. 8.2(a) and 8.2(b) is replaced by the full circle in Fig. 8.2(c), because the lower half of it for the vector $\boldsymbol{\delta}_1$ of the first prism and the upper half for the vectors $\boldsymbol{\delta}_2$ of the second prism.

Figure 8.2. illustrates the method of geometric construction and Fig. 8.3 shows the final results, in which the parallelogram $\square OAB'C$ shows the relationship between the key parameters $\boldsymbol{\delta}_1$, $\boldsymbol{\delta}_2$ and Φ, that provides the basis to develop an analytic first-order solution to the inverse problem.

8.1.2 First-order analytical solutions to the inverse problem

Attention is now concentrated on the triangle $\Delta OB'C$, that is an isosceles triangle with three edges shown by δ_2, Φ and δ_1 (where $\delta_1 = \delta_2 = \delta$.) opposing to the three internal angles $(\Delta\theta)_0/2$, $(\Delta\theta)_0/2$ and $180° - (\Delta\theta)_0$ at the three vertices O, B′ and C, respectively. Making use of the sine law, we obtain from $\Delta OB'C$ that

$$\frac{\Phi}{\sin[180^o - (\Delta\theta)_1]} = \frac{\delta}{\sin[(\Delta\theta)_1/2]}.$$

Re-arranging terms, we find the angle of relative rotation of the two prisms, given by

$$(\Delta\theta)_1 = \pm 2 \arccos\left(\frac{\Phi}{2\delta}\right), \tag{8.1}$$

where "+" for the case shown in Fig. 8.2(a) and "−" for 8.2(b). For the case shown in Fig. 8.2(c), we may use either "+" or "−" with an additional requirement of $\theta_1 = -\theta_2$.

Equation (8.1) and Fig. 8.3(a) show the rotation of the second prism an angle $(\Delta\theta)_1$ to meet the requirement of the altitude angle Φ, and Fig. 8.3(a) shows a co-rotation the two prisms an angle $\Theta - \psi_0$ to meet the requirement of the altitude angle Θ.

8.2 Third-Order Approximation to the Inverse Problem

Attention is now turned to the third-order inverse solution of precise pointing, i.e., the problem of steering a laser beam to a specific point of altitude Φ and

azimuth Θ within the angular range of the system (see, e.g., [7.2, 7.3,7.4, 7.5] and references cited therein).

The altitude Φ is the angular separation of the point of interest (i.e., the target) and the z axis, whereas the azimuth angle Θ is the angular separation of the point of interest (i.e., the target) to the axis of reference, say, the x axis (see, Fig. 8.1). The altitude of the target should be in the angular range [$\phi_{\min}$, $\phi_{\max}$] of the Risley prism pair, i.e.,

$$\varphi_{\min} \le \Phi \le \varphi_{\max} \quad \text{and,}$$

where $\varphi_{\min}$ and $\varphi_{\max}$ are the minimum and maximum angles of deviation by the prisms as shown in Figs. 7.10 and 7.13.

To consider a concise and closed-form solution to the inverse problem within the accuracy of the third-order theory of the Risley-prism-based beam steering system [7.13], we return to the expressions of the direction cosines $\left(k_{22}^{(r)},\ l_{22}^{(r)},\ m_{22}^{(r)}\right)$ in Eq. (7.14) and re-write them in the form

$$\left.\begin{aligned} k_{3\text{rd}} &= -(\delta_1 \cos\theta_1)\kappa_1 - (\delta_2 \cos\theta_2)\kappa_2, \\ l_{3\text{rd}} &= -(\delta_1 \sin\theta_1)\kappa_1 - (\delta_2 \sin\theta_2)\kappa_2, \\ m_{3\text{rd}} &= -1 + \frac{\delta_1^2}{2} + \frac{\delta_2^2}{2} + \delta_1\delta_2 \cos(\Delta\theta) \end{aligned}\right\}, \tag{8.2}$$

where $\Delta\theta = \theta_2 - \theta_1$, and

$$\left.\begin{aligned} \kappa_1 &= 1 + \frac{3 - n_1}{6n_1(n_1 - 1)^2}\delta_1^2, \\ \kappa_2 &= 1 + \frac{\delta_1^2}{2n_2} + \frac{3n_2 - 1}{6(n_2 - 1)^2}\delta_2^2 + \frac{\delta_1\delta_2 \cos(\Delta\theta)}{n_2 - 1} \end{aligned}\right\}.$$

To steer the beam into the direction specified by (Φ, Θ), the first step is to rotate the second prism Π_2 and keep the first prism Π_1 at rest until the desired altitude is achieved, i.e.,

$$\cos\Phi = -m_{3\text{nd}} = 1 - \frac{\delta_1^2}{2} - \frac{\delta_2^2}{2} - \delta_1\delta_2 \cos(\Delta\theta)_0, \tag{8.3}$$

where $(\Delta\theta)_0 = \theta_2 - \theta_1$ represents the angle of relative rotation of the two prisms, which can be obtained from Eq. (8.3) as

$$\cos(\Delta\theta)_0 = \frac{2(1 - \cos\Phi) - (\delta_1^2 + \delta_2^2)}{2\delta_1\delta_2} \tag{8.4}$$

It is worth of noting that $\Delta\theta = \theta_2 - \theta_1$ in Eq. (8.2) is a variable, whereas $(\Delta\theta)_0$ in Eq. (8.3) is a parameter depending on the altitude of the target.

8.2.1 Beam steering angle of a Risley prism pointer

Figures 8.2. and 8.3 show the prediction of the first-order theory about the maximum beam steering angle of Risley prism required by range of precise pointing, and we found that is $\Phi \leq \delta_1 + \delta_2$. The following discussion considers the same problem predicted by the third-order theory.

Equation (8.4) shows the maximum beam steering angle of Risley prism is obtained when the angle of relative rotation of the two prisms $(\Delta\theta)_0 = 0$, i.e., when

$$\frac{2(1-\cos\Phi) - (\delta_1^2 + \delta_2^2)}{2\delta_1\delta_2} = 1 \tag{8.5a}$$

After some rearranging, Eq. (8.5a) becomes

$$\bar{\delta} \geq \sin(\Phi/2), \quad \text{or } 2\sin(\Phi/2) \leq \delta_1 + \delta_2, \tag{8.5b}$$

where $\bar{\delta} = (\delta_1 + \delta_2)/2$, is the arithmetic mean of the power of the two prisms. Comparing to the first-order prediction shown above, Eq. (8.5b) contains a third-order term if we consider the expansion of $\sin x = x - x^3/6$.

Assume the use of two identical prisms, i.e., if $n_1 = n_2 = n$ and $\alpha_1 = \alpha_2 = \alpha$, we may insert Eq. (7.1) into Eq. (8.5b) and obtain

$$\alpha \geq \frac{\sin(\Phi/2)}{n-1} \tag{8.5c}$$

Table 8.1 shows a numerical comparison of the accuracy of the third-order theory with the predictions of the exact solution obtained from the data for plotting the curves labeled A-1 in Figs. (7.13a) and (7.13b) about the total deviation angle $\Delta\varphi_m$ as a function of the prism angle α when $\Delta\varphi_m \geq \Phi = 10°$, 20°,..., 40°. It is seen when the wedge angle $\alpha \sim 10°$ the difference between the two theories is 2.3% when $n = 1.5$. Difference between them increases significantly to 17.8% when $\alpha \sim 30°$.

8.2.2 Two-step method for the inverse solution of Risley prism pointer

The curves in Fig. 8.4(a) are plotted from Eq. (7.4b) to show the one-to-one correspondence between the altitude angle Φ of the beam in the direction pointing to the target and the relative rotation angle $(\Delta\theta)_0$ of the two prisms in systems that have two identical prisms of index $n_1 = n_2 = 1.5$ and prism angle $\alpha_1 = \alpha_2 = 2.5°, 5.0°, \ldots, 10°$.

Equation (8.3) is the central equation of step 1 in the two-step method when applied to third-order approximation. After step 1, the orientations of the two prisms are at $\theta_1 = 0$ and $\theta_2 = (\Delta\theta)_0$, and the beam is pointing to a point in the direction specified by (Φ, ψ_0), where ψ_0 is an intermediate result, not the final requirement about the target azimuth angle Θ. The central

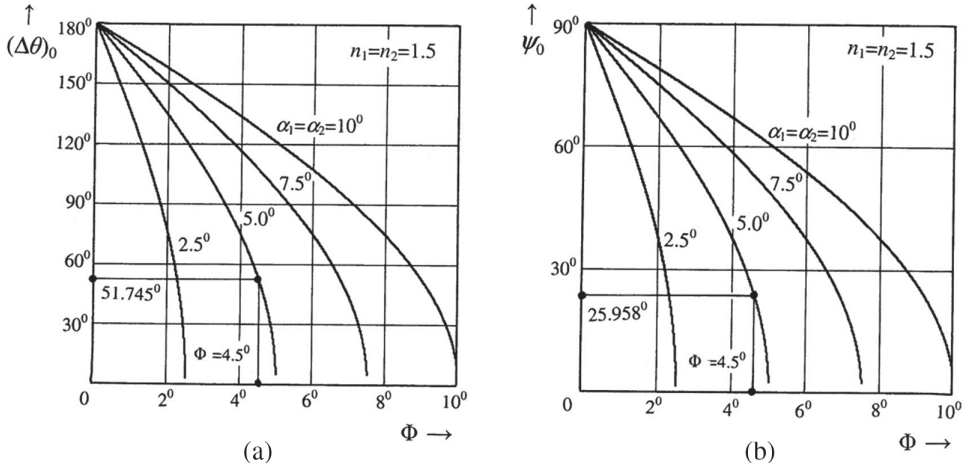

Figure 8.4 Curves plotted within the accuracy of the third-order theory for the Risley prism pairs using two identical components of index $n_1 = n_2 = 1.5$ and different apex angle $\alpha_1 = \alpha_2 = 2.5°, 5.0°, \ldots, 10°$. Illustrating the two-step method for the inverse solution of steering a laser beam to highlight the point specified by the altitude Φ and azimuth Θ. (a) Curves, plotted from Eq. (7.4) for the use in the first step of the two-step method, show the dependence of the relative rotation angle $(\Delta\theta)_0$ of the two prisms on the altitude angle Φ of the point of interest. This method keeps the prism Π_1 at rest, while rotating the prism Π_2 to the angle $(\Delta\theta)_0$ to steer the beam to the direction specified by the altitude angle Φ. (b) The two prisms are co-rotated by an angle $\Theta - \psi_0$ to steer the beam to the target. The angle ψ_0 is the azimuth of the beam after the first step. The curves of ψ_0 are plotted from Eq. (7.8) for the use in the second step of the two-step method.

equation of step 2 is therefore a determination of the angle ψ_0, from where a co-rotation of the two prisms (i.e., no relative motion between them) from ψ_0 to Θ to accomplish target pointing. From Fig. 8.1, we can express ψ_0 in the form

$$\psi_0 = \arctan\left(\frac{l_{3\text{rd}}}{k_{3\text{rd}}}\right)_{\substack{\theta_1=0,\\ \theta_2=(\Delta\theta)_0}} . \tag{8.6}$$

After substituting from Eqs. (8.2) into Eq. (8.6), we find

$$\left(\frac{l_{3\text{rd}}}{k_{3\text{rd}}}\right)_{\substack{\theta_1=0,\\ \theta_2=(\Delta\theta)_0}} = \frac{\kappa_{20}\sqrt{4\delta_1^2\delta_2^2 - [2(1-\cos\Phi) - (\delta_1^2+\delta_2^2)]^2}}{2\kappa_1\delta_1^2 + \kappa_{20}[2(1-\cos\Phi) - (\delta_1^2+\delta_2^2)]}, \tag{8.7}$$

where

$$\kappa_{20} = \kappa_2\Big|_{\substack{\theta_1=0,\\ \theta_2=(\Delta\theta)_0}} = 1 + \frac{\delta_1^2}{2n_2} + \frac{3n_2 - 1}{6(n_2 - 1)^2}\delta_2^2 + \frac{2(1 - \cos\Phi) - (\delta_1^2 + \delta_2^2)}{2(n_2 - 1)}. \tag{8.8}$$

Again, substituting Eq. (8.8) into Eq. (8.7) and then into Eq. (8.6) and after discarding all terms of an order higher than δ^3, there remains

$$\psi_0 = \arctan\left[\frac{(n_2 - \cos\Phi)\sqrt{4\delta_1^2\delta_2^2 - [2(1 - \cos\Phi) - (\delta_1^2 + \delta_2^2)]^2}}{(n_2 - 1)\delta_1^2 + (n_2 - \cos\Phi)[2(1 - \cos\Phi) - (\delta_1^2 + \delta_2^2)]}\right], \tag{8.9}$$

which is plotted in Fig. 8.4(b) under the same conditions set for plotting the curves in Fig. 8.4(a).

In the second step of the two-step method, the beam from the system traces out the surface of a cone with a half-vertex angle Φ in the free space. The center of the target in the direction specified by (Φ, Θ) must be a point on the cone surface and can be reached after rotating the two prisms together by an angle $\Theta - \psi_0$. This means the final orientations of the two prisms are given, respectively, by

$$\theta_1 = \Theta - \psi_0 \quad \text{and} \quad \theta_2 = \theta_1 - (\Delta\theta)_0 = \Theta - \psi_0 - (\Delta\theta)_0. \tag{8.10}$$

To this point a case study may be helpful to show the use of the two-step method and the accuracy of the inverse solution obtained from the third-order theory.

Consider a Risley prism pair with two identical glass prisms of index $n = 1.5$ and prism angle $\alpha = 5°$, which is required to steer a laser beam to the target in the direction at an altitude $\Phi = 4.5°$ and azimuth $\Theta = 120°$.

In the first step of the two-step method, we insert $\Phi = 4.5°$ into Eq. (8.7) and obtain the relative rotation angle $(\Delta\theta)_0 = 51.745°$. However, computed result of Eq. (8.9) reveals that the beam is now pointing into the point in the direction specified by altitude $\Phi = 4.5°$ and azimuth $\psi_0 = 25.958°$.

The second step is a co-rotation of the two prisms from azimuth angle $\psi_0 = 25.958°$ to the required target azimuth $\Theta = 120°$. Finally, orientations of the two prisms, defined by Eq. (8.10), reach the following levels:

$$\theta_1 = \Theta - \psi_0 = 120° - 25.958° = 94.042°,$$

and

$$\theta_2 = \theta_1 + (\Delta\theta)_0 = 94.042° + 51.745° = 145.787°.$$

To show the accuracy of the third-order theory for the inverse problem and also the effectiveness of the method described above, we may insert the computed results of $\theta_1 = 94.042°$ and $\theta_2 = 145.787°$ back into Eq. (7.14) for the solutions from Eqs. (8,11a) and (8.13aa) of the direction cosines, and then the altitude $\Phi = 4.523°$ and the azimuth $\psi_0 = 25.961°$, which are very close to their values of $\Phi = 4.5°$ and $\psi_0 = 25.958°$ obtained from Eqs. (8.6) and (8.6).

8.3 Closed-Form Analytic Inverse Solution of Two-Element Risley Prism Pointers in different configurations

This Section considers the closed-form analytical solutions for the inverse problem of precise pointing by Risley prism pairs in four different configurations (see, e.g., Fig. 7.7). Results of this section have been considered as exact due to the use of the Snell's law in vector form for a non-paraxial ray trace of a ray through a prism pair without relying on the approximate technique such as $\sin x \cong x - x^3/6$, which implies the applicability of the closed-form analytical solutions to wedge prisms of different wedge angles; however, the exactness of the raytracing results was questioned because of the ignorance of the influence of prism thickness d_1 and d_2 and the air gap d_{air} between them on the pointing accuracy. In response to this question, the consequence of ignoring the contributions of (d_1, d_2, d_{air}) will be evaluated quantitatively in Section 8.5 that reveals the results of in this Section are valid for precise detecting and tracking targets in both the near-and far-fields if their linear dimensions are larger than that of a prism thickness.

8.3.1 Closed-form noniterative inverse solutions of two-element Risley prism pointers in different configurations

To steer the beam to the direction specified by the altitude angle Φ and the azimuth angle Θ has been shown in Fig. 8.1. The first step is to keep the prism Π_1 stationary, say, at $\theta_1 = 0$, and rotate the second prism Π_2 until the desired altitude Φ is achieved, i.e., a rotation of Π_2 relative to Π_1 until the following condition for system in Group A [see, Figs. 7.7(a) and (b)] is satisfied:

$$\cos\Phi = -m_{2\text{A}} = -(a_2 - a_3\cos\alpha_2), \tag{8.11a}$$

and for a system in Group B [see, Figs. 7.7(c) and (d)], we have the condition:

$$\cos\Phi = -m_{2\text{B}} = \sqrt{1 - n_2^2 + (b_2 + b_3\cos\alpha_2)^2}. \tag{8.11b}$$

The a- and b-parameters in the above two expressions are from Eqs. (7.31) and (7.32), respectively.

After substituting from Eqs. (T7.3.3) and (T7.3.5) in Table 7.3 for the coefficient a_2 and a_3 into Eq. (8.11a), we obtain an expression containing the relative rotation angle $(\Delta\theta)_0 = \theta_2 - \theta_1$ of the two prisms. Solving this expression for the angle $(\Delta\theta)_0$, we find that

$$(\Delta\theta)_0 = \pm\arccos\left(\frac{1}{a_1\tan\alpha_2}\left\{a_2+\frac{1}{2(a_2+\cos\Phi)}\left[1-n_2^2-\left(\frac{a_2+\cos\Phi}{\cos\alpha_2}\right)^2\right]\right\}\right), \tag{8.12a}$$

in which the "±" implies that $(\Delta\theta)_0$ may be expressed either as $\theta_2 - \theta_1$ or as $\theta_1 - \theta_2$, i.e., there is no effect if the two prisms exchange their angular positions. This reciprocity is a result of ignorance of thickness of the two prisms and the width of the air gap between them, which implies Eqs. (8.12a) and (8.12b) are valid only in the far region of the scan field.

For the prism systems in Group B, the angle $(\Delta\theta)_0$ can be obtained by substituting from Eqs. (T7.4.3) and (T7.4.5) in Table 7.4 for the coefficients b_2 and b_3 into Eq. (8.11b) to obtain an expression that contains the angle $(\Delta\theta)_0$, which can be solved as

$$(\Delta\theta)_0 = \pm\arccos\left(\frac{1}{b_1\tan\alpha_2}\left\{b_2+\frac{1}{2\left(-b_2\pm\sqrt{n_2^2-\sin^2\Phi}\right)}\left[1-n_2^2+\left(\frac{-b_2\pm\sqrt{n_2^2-\sin^2\Phi}}{\cos\alpha_2}\right)^2\right]\right\}\right). \tag{8.12b}$$

Here the "±" sign appeared again on the right sides that implies for Risley beam director in either A- or B-configuration, there are always two possible prism orientations if target in the far-region of the scan field.

If Eqs. (8.12a) and (8.12b) are considers as definitions of functions of $\Delta\theta = f(\Phi)$, then the inverse functions $\Phi = f^{-1}(\Delta\theta)$ are found as

$$\Phi = \arccos\left\{-a_2+\left[g(a_1,\, a_2;\, (\Delta\theta)_0)\pm\sqrt{g^2(a_1,\, a_2;\, (\Delta\theta)_0)-n_2^2+1}\right]\cos\alpha_2\right\}, \tag{8.12c}$$

and

$$\Phi=\arcsin\sqrt{n_2^2-\left\{-b_2+\left[g(b_1,b_2;(\Delta\theta)_0)\ \pm\sqrt{g^2(b_1,b_2;(\Delta\theta)_0)+1-n_2^2}\right]\cos\alpha_2\right\}^2},\tag{8.12d}$$

where $g(a_1, a_2; (\Delta\theta)_0) = a_2\cos\alpha_2 - a_1\sin\alpha_2\cos(\Delta\theta)_0$ and $(0 \le \Phi \le \pi)$.

After the desired altitude is achieved, the beam points to a point in the direction specified by the angles (Φ, ψ_0). For systems in Group A, the azimuth displacement ψ_0 found in the first step of the two-step method, given by

$$\psi_0=\arctan\left(\frac{l_{2A}}{k_{2A}}\right)_{\substack{\theta_1=0,\\ \theta_2=(\Delta\theta)_0}}=\arctan\left[\frac{(a_2+\cos\Phi)\tan\alpha_2\sin(\Delta\theta)_0}{a_1+(a_2+\cos\Phi)\tan\alpha_2\cos(\Delta\theta)_0}\right]+C,\tag{8.13a}$$

where $C = 0$ when $(k_A)_{\substack{\theta_1=0,\\ \theta_2=(\Delta\theta)_0}} \ge 0$ and $C = \pi$ when $(k_A)_{\substack{\theta_1=0,\\ \theta_2=(\Delta\theta)_0}} < 0$.

Similarly, for prism systems in Group B, we have

$$\begin{aligned}\psi_0 &= \arctan\left(\frac{l_{2B}}{k_{2B}}\right)_{\substack{\theta_1=0,\\ \theta_2=(\Delta\theta)_0}}\\ &= \arctan\left[\frac{\left(b_2 \mp \sqrt{n_2^2-\sin^2\Phi}\right)\tan\alpha_2\sin(\Delta\theta)_0}{b_1+\left(b_2 \mp \sqrt{n_2^2-\sin^2\Phi}\right)\tan\alpha_2\cos(\Delta\theta)_0}\right]+C.\end{aligned}\tag{8.13b}$$

The second step in the two-step method is a co-rotation of the prisms Π_1 and Π_2 about the axis of the system until the desired azimuth Θ is reached. The final rotation angles of Π_1 and Π_2 are given, respectively, by

$$\theta_1 = \Theta - \psi_0 \quad \text{and} \quad \theta_2 = \theta_1 + (\Delta\theta)_0 = \Theta - \psi_0 + (\Delta\theta)_0.\tag{8.14a}$$

If the initial phase angles of Π_1 and Π_2 are θ_{10} and θ_{20}, then Eq. (8.14a) should be read as

$$\theta_1 - \theta_{10} = \Theta - \psi_0 \quad \text{and} \quad \theta_2 - \theta_{20} = \theta_1 - \theta_{10} + (\Delta\theta)_0 = \Theta - \psi_0 + (\Delta\theta)_0.\tag{8.14b}$$

It is worth of noting the restriction on the altitude in Eqs. (8.12)–(8.14), i.e.,

$$\varphi_{\max} \ge \Phi \ge \varphi_{\min},$$

where $\varphi_{\max}$ and $\varphi_{\min}$ are shown in Figs. 7.9 and 7.13.

Substituting from $(\Delta\theta)_0 = 0$ and π into Eqs. (8.12c) and (8.12d), we obtain $\Phi = \varphi_{\max}$ and $\varphi_{\min}$ for Risley prisms in the A and B configurations, respectively, i.e.,

$$\varphi_{\max} = \Phi|_{(\Delta\theta)_0=0} \quad \text{and} \quad \varphi_{\min} = \Phi|_{(\Delta\theta)_0=0}. \tag{8.15}$$

As the first numerical example, we consider a glass prism system of $n_1 = n_2 = n = 1.5$ and $\alpha_1 = \alpha_2 = \alpha = 10°$ in Risley prisms in A-1 configuration and obtain from Eqs. (8.12c) and (8.15) that $\varphi_{\max} = 10.268°$ and $\varphi_{\min} = 0$ and. Further, for silicon prisms $n_1 = n_2 = n = 4.0$ and $\alpha_1 = \alpha_2 = \alpha = 8°$, we obtain $\varphi_{\max} = 67.489°$ and $\varphi_{\min} = 0$ (no blind zone).

As the second numerical example, we consider glass prism system of $n_1 = n_2 = n = 1.5$ and $\alpha_1 = \alpha_2 = \alpha = 10°$ in Risley prisms in B-1 configuration and obtain $\varphi_{\max} = 10.064°$ and $\varphi_{\min} = 0.065°$; for silicon prisms $n_1 = n_2 = n = 4.0$ and $\alpha_1 = \alpha_2 = \alpha = 8°$, we have $\varphi_{\max} = 57.194°$ and $\varphi_{\min} = 0.916°$. Since the B-1 configuration is mirror asymmetric, the angular size of the bind zone is shown here by the values of $\varphi_{\min} \neq 0$ as discussed in Subsection 7.3.2.

8.3.2 Comparison of the predictions by theories with different degrees of accuracy

Consider an error-free Risley prism pair steers a laser beam into the direction of a target in the far-region of the scan field specified by the altitude and azimuth (Φ, Θ). The far field exact solution to this pointing problem predicts the angular positions of two prisms

$$(\theta_1)_{\text{Exact}} \quad \text{and} \quad (\theta_2)_{\text{Exact}},$$

whereas the third-order theory in Section 8.1 predicts the positions of the two prisms in the same system

$$(\theta_1)_{3\text{rd}} \quad \text{and} \quad (\theta_2)_{3\text{rd}}\,.$$

We are looking for the difference of the data listed above, i.e.,

$$(\Delta\theta)_I = (\theta_1)_{\text{Exact}} - (\theta_1)_{3\text{rd}} \tag{8.16a}$$

and

$$(\Delta\theta)_{II} = (\theta_2)_{\text{Exact}} - (\theta_2)_{3\text{rd}}. \tag{8.16b}$$

Making use of the relationships between (Φ, Θ) and (θ_1, θ_2) given by Eqs. (8.9) and (8.13), we may express $(\Delta\theta)_{\text{I}}$ and $(\Delta\theta)_2$ further as

$$(\Delta\theta)_I = \Theta - (\psi_0)_{\text{Exact}} - [\Theta - (\psi_0)_{3\text{rd}}] = -(\psi_0)_{\text{Exact}} + (\psi_0)_{3\text{rd}}$$

and

$$(\Delta\theta)_{II} = (\Delta\theta)_{I+}[(\Delta\theta)_0]_{\text{Exact}} - [(\Delta\theta)_0]_{\text{3rd}},$$

where the expressions relating to $(\psi_0)_{\text{Exact}}$ and $(\psi_0)_{\text{3rd}}$ are given by Eqs. (8.13a), (8.13b), and (8.9), respectively, whereas the expressions of $[(\Delta\theta)_0]_{\text{Exact}}$ and $[(\Delta\theta)_0]_{\text{3rd}}$ can be found from Eqs. (8.12a), (8.12b) and (8.4b), respectively. These equations show that $(\Delta\theta)_{\text{I}}$ and $(\Delta\theta)_{\text{II}}$ are determined by the altitude Φ only and the azimuth Θ is a factor independent from the comparison of the results predicted by different theories.

To understand this situation, let us consider the following viewpoints:

- The azimuth Θ is the factor that works only in the second step of the two-step method, which is a step with a rigid motion of the two prisms as a whole, i.e., no change of the relative position of all points in the two prisms,
- Since the incidence is assumed parallel and coincided with the axis of rotation, the ray path inside the Risley prism pair remains the same regardless of the co-rotation of the two prisms to an azimuth Θ with any value,
- Since ray path remains unchanged, the predictions of different theories remain the same.

Based on the above viewpoints, we may assume the azimuth angle $\Theta = 0$ for simplicity. After that, our attention is concentrated to the evaluation of $(\Delta\theta)_{\text{I}}$ and $(\Delta\theta)_{\text{II}}$ within the region of $(0, \Delta\varphi_{\text{m}})$, where $\Delta\varphi_{\text{m}} = \varphi_{\max} - \varphi_{\min}$ is the amplitude of ray deviation [see Fig. 7.13].

If the point of interest is at $(x_1, y_1, -P)$ in the Cartesian coordinates system shown in Fig. 8.1, we have

$$x_1 = P\tan\Phi \quad \text{and} \quad y_1 = 0. \tag{8.17}$$

Comparison of point accuracy starts from substituting $(\Phi, \Theta = 0)$ into the third-order Eqs. (8.6) – (8.10) to yield the rotation angles $(\theta_1)_{\text{3rd}}$ and $(\theta_2)_{\text{3rd}}$ of the two prisms, which will be inserted into Eqs. (7.31), (T7.3.1) and (T.3.2) in Table 7.3 (for exact theory expressions) to find the point $(x_2, y_2, -P)$, i.e., the point where the laser beam hits the point of interest on the plane at $z = -P$, as predicted by the exact theory under the condition that the two prisms are in the same angular positions as obtained in the first step for the third-order theory.

The distance d between the two points $(x_1, y_1, -P)$ and $(x_2, y_2, -P)$ represents the pointing error that can be evaluated by the following formula:

$$d = \sqrt{(x_2 - x_1)^2 + (y_2 - y_1)^2}, \tag{8.18}$$

Because $(x_2, y_2, -P)$ is proportional to direction cosines (k_A, l_A, m_A) of the ray emerging from the system, we may obtain (x_2, y_2) from the proportional allocation formula in the form

$$\frac{x_2}{k_{2A}} = \frac{y_2}{l_{2A}} = \frac{-P}{m_{2A}}, \tag{8.19}$$

where (k_A, l_A, m_A) can be found from Eq. (7.31) and should be evaluated at the point of $\theta_1 = (\theta_1)_{3rd}$ and $\theta_2 = (\theta_2)_{3rd}$. After substituting from Eqs. (8.17) and (8.19) into Eq. (8.18), we find

$$\frac{d}{P} = \sqrt{\left[\left(\frac{k_{2A}}{m_{2A}}\right) + \tan\Phi\right]^2 + \left(\frac{l_{2A}}{m_{2A}}\right)^2}\Bigg|_{\substack{\theta_1=(\theta_1)_{3rd},\\ \theta_2=(\theta_2)_{3rd}}}. \tag{8.20}$$

Figure 8.5 is plotted from Eq. (8.20) to show the normalized pointing error d/P as a function of the normalized altitude $\Phi/\Delta\varphi_m$ with the prism opening angle α as a parameter, where the notation $\Delta\varphi_m = \varphi_{max} - \varphi_{min}$ represents the amplitude of ray deviation angle of the pointing device and has been plotted in Fig. 7.13 from Eq. (7.37).

More specifically, the parameters of the two identical prisms are $n = 1.5$ for glass prisms in Fig. 8.5(a) and $n = 4.0$ for silicon prisms in Fig. 8.5(b), both are plotted for the same prism angle of $\alpha = 1°$; $2°$, $5°$ and $10°$. We may find the value of $\Delta\varphi_m$ from the curve labeled A-1 in Fig. 7.13 or from Eq. (7.37) when the value of α is given.

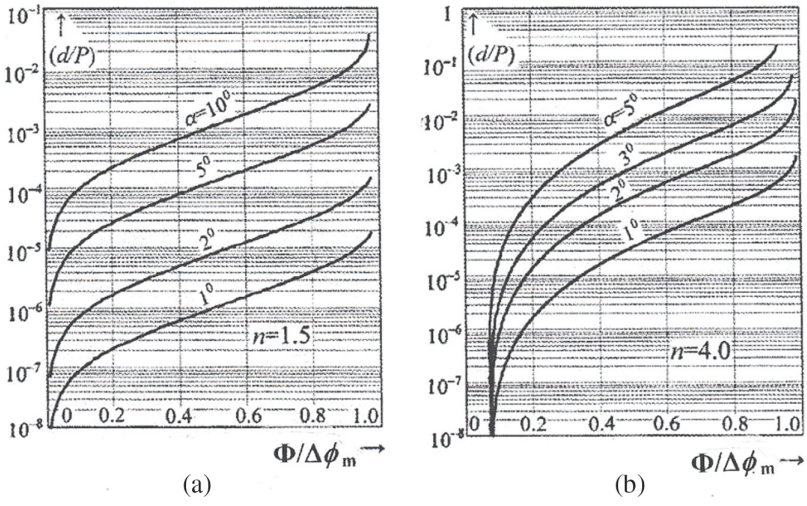

Figure 8.5 Pointing error as the third-order theory compared to the exact solution to the inverse problem of the Risley prism pairs in the A-1 configuration of two identical prisms of (a) $n = 1.5$ and (b) $n = 4.0$. The amplitude of ray deviation angle $\Delta\varphi_m = \varphi_{max} - \varphi_{min}$ from Fig. 7.13.

Figure 8.5. shows that the difference between the predictions of the third order theory and the exact solution falls in the region $10^{-5} < d/P < 10^{-4}$ when the altitude of the point of interest $\Phi \leq 2°$. A similar situation can be seen in Fig. 8.5(b) plotted under the conditions of systems that use silicon prisms of $n = 4$ with prism angles of $\alpha = 1°$, 2°, 3° and 5°.

8.3.3 Pointing stability and agility

We show pointing accuracy through a case study, in which a laser beam is required to be steered into the direction specified by the altitude $\Phi = 4.5°$ and azimuth $\Theta = 120°$. The prism system contains two identical components of index $n = 4.0$ and prism angle $\alpha = 5°$. If this system is in the A-1 (i.e., TV-VT) configuration, the first step is to obtain the relative rotation angle $(\Delta\theta)0 = 162.768°$ from Eq. (8.12a), and then from Eq. (8.13a) we may obtain the azimuthal angular displacement $\psi_0 = 81.578°$ introduced by the rotation of Π_2 relative to Π_1. The second step is a co-rotation of Π_1 and Π_2 to bring the azimuth angle from ψ_0 to the requirement at $\Theta = 120°$. After the two steps, the final orientations of the two prisms are given by

$$\theta_1 = \Theta - \psi_0 = 120° - 81.578° = 38.422°$$

and

$$\theta_2 = \theta_1 + (\Delta\theta)_0 = 38.422° + 162.768° = 201.190°.$$

Under the same conditions of system configuration and characterization, the predictions of the first-, the third-order and the exact theories are shown in Table 8.2.

The angular difference between the predictions of different theories is as small as 0.025%. This is not surprising, because under the condition of $\alpha \leq 5°$ the third-order theory predicts results with high accuracy as shown numerically in the Section 8.1. The surprising issue is that a small angular error may cause a huge position-finding error if the target is located hundreds of mile away, e.g., at 500 km the position error will be ~125 m, which may be much larger than the maximum linear dimension of the target.

Pointing to a remote target, the important factor is pointing stability, which is a measure of how much the beam position drifts from the ideal target over time. Beam position fluctuations in a laser may be introduced by mechanical vibrations and/or by thermal effects on the beam position. The beam-pointing stability of commercial laser products is often quantitatively specified. Unfortunately, such specifications are often not precise enough and need careful verification. [8.9, 8.10]

The two-step method [8.1] can be summarized as a relative rotation followed by a co-rotation of the two prisms for the purpose to steer laser beam into the direction specified by the altitude and azimuth (Φ, Θ). Since no

restriction has been imposed on the precedence of relative rotation and we may rotate one prism first and keep another one at rest or to rotate both of them simultaneously for the purpose to reduce the time of prism position adjustment to a minimum.

To describe different modes of relative rotation of the two prisms, we use a parameter κ and the rotation of prism Π_1 is specified by $\theta_1 = -\kappa(\Delta\theta)_0$ and $\theta_2 = (1 - \kappa)(\Delta\theta)_0$ for prism Π_2. Specifically, $\kappa = 0$ implies Π_2 moves first while Π_1 at rest, $\kappa = 1$ implies the other way round and $\kappa = 0.5$ for rotating the two prisms simultaneously to the angles $\mp 0.5(\Delta\theta)_0$.

Graphic solutions shown in Figs. 8.2 and 8.3 reveal that the motion mode described by $\kappa = 0$ is the most suitable for azimuth $\Theta < 180°$, $\kappa = 0.5$ for azimuth $\Theta < 1\ 0°$ and $\kappa = 1.0$ for azimuth $\Theta > 180°$.

If computed results are more convincing, let us return the case example in subsection 8.2.3, i.e., the laser beam is required to be steered into the direction specified by the altitude $\Phi = 4.5°$ and azimuth $\Theta = 120°$. The prism system is built up by two identical components of index $n = 4.0$ and opening angle $\alpha = 5°$. For the case of $\kappa = 0$, the main results can be summarized as

- Assume $\theta_1 = \theta_2 = 0°$ (two prisms at rest positions).
- After the first rotation of the prism Π_2 an angle $(\Delta\theta)_0$ relative to Π_1: $\theta_1 = 0°$ and we found $\theta_2 = 162.768°$;
- After the second rotation of prisms Π_1 and Π_2 together an angle $\Theta - \psi_o = 38.422°$, and we obtain $\theta_1 = 38.422°$ and $\theta_2 = 201.190°$.

If the azimuth Θ increases from 120° to 240° (or, −120°), then the second rotation angle increases drastically from 38.422° to 158.422°. However, we may change the motion mode from $\kappa = 0$ to $\kappa = 1.0$ to reduce the second rotation angle and obtain the second rotation angle $\Theta - \psi_o = -120° - (-81.189°) = -38.811°$ with the prisms' orientations at $\theta_1 = -201.579°$ and $\theta_2 = -38.811°$.

Finally, If the azimuth Θ decreases from 120° to 10°, then the second rotation angle changes from 38.422° to −71.578°. However, we may change the motion mode from $\kappa = 0$ to $\kappa = 0.5$ to reduce the second rotation angle and obtain the second rotation angle $\Theta - \psi_o = 10° - (0.195°) = 9.805°$ with the prisms' orientations at $\theta_1 = -71.578°$ and $\theta_2 = 91.189°$.

Appendix G shows a one-step method that may considerably improve the computational efficiency and reduce the round up error in data processing.

8.3.4 Symmetric and asymmetric Risley prism configurations and their influence on precise pointing

Figure 7.7 shows the four different configurations of Risley prism pairs, which are divided into A and B Groups based on the VT or the TV arrangement of their second prism in the system. From the analysis in Subsection 7.3.1, we

found that the structures of the scan fields produced by the A-1 and A-2 configurations in the Group A can be described by expressions in semilar form as summarized in Eq. (7.31) and Table 7.3; and Eq. (7.32) and Table 7.4 are found for the B-1 and B-2 configurations in the Group B. Classification of Risley prism pairs in different configuration becomes possible due mainly to the fact that the function of the first prism in the system is the generation of a circular cone around the mechanical axis; generation of different scan patterns relies on the power, rotation speed and direction of the second prism relative to the first one.

However, in the application of Risley prism pairs to precise pointing, we have to consider another kind of principle for classification of Risley prism pairs in different configurations, i.e., dividing according to their mirror symmetric properties in reference to the central line of the system when the two prisms in the positions specified by the relative rotation angle $\Delta\theta = \theta_2 - \theta_1 = 0, \pm 360°, \ldots$.

Specifically, the A-1 and B-2 configurations in Fig. 7.7 are mirror symmetry (also known as line symmetry or reflectional symmetry), because there is a line $\overline{MM}$ going through the center of air gap of the system, which divides the system into two pieces which are the mirror images of each other. Furthermore, it is known from Subsection 7.2.3 that the Risley prism pairs are equivalent to a single prism of variable power, and the power is zero when the apexes of the prisms are opposed, i.e., when orientation specified by the relative rotation angle $\Delta\theta = \pm 180°, \pm 540°, \ldots$. Under this condition, the Risley prism pairs reduce to a sandwiched configuration with plane-parallel plates with a uniform air gap between the plates, as shown by the dashed line rectangular and parallelogram boxes in Fig. 8.6(a).

Analysis of refraction by plane-parallel plate in the air reveals that a single ray traversing such an optical element with surfaces in parallel to each other (see, e.g., Section 2.3 in [7.19]), the ray emergent from the system is parallel to its original direction. This implies the rays of incidence and emergence are in the same direction, i.e., there is no ray deviation or $\varphi_{\min} = 0$, or, more directly, the Risley prism pairs in the A-1 and B-2 configurations are able for pointing targets specified by the altitude from $\Phi = \varphi_{\min} = 0$ to $\Phi = \varphi_{\max}$, whereas the A-2 and B-1 in Fig. 7.7(b) are not in the image symmetric configurations when $\Delta\theta = 0, \pm 360°, \ldots$ and they are non-parallel plates when $\Delta\theta = \pm 180°, \pm 540°, \ldots$ [see the non-rectangular boxes enclosed by the dashed lines in Fig. 8.6(b)]. As a consequence of refraction by non-parallel plates, the Risley prism pairs in the A-2 and B-1 configurations are not able for pointing targets specified by the altitude from $\Phi = 0$ to $\Phi = \varphi_{\min}$, but able for pointing targets only in the annular zone specified by the altitude from $\Phi = \varphi_{\min}$ (>0) to $\Phi = \varphi_{\max}$. Since no scan field in the zone from $\Phi = 0$ to $\Phi = \varphi_{\min}$, where is, therefore, known as the pointing dead zone, as summarized in Fig. 8.6.

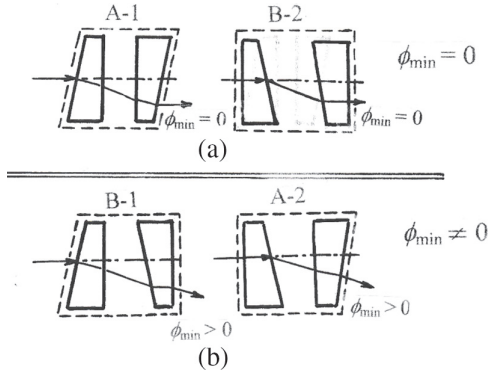

Figure 8.6 Ray path diagrams showing two groups of Risley prism pairs according to their ray deviation angle φ_{min} when the two prisms opposed. (a) $\varphi_{min} = 0$ for A-1 and B-2 configurations in group of no pointing dead zone, and (b) $\varphi_{min} > 0$ for A-2 and B-1 configurations in the group with pointing dead zone.

The curves in Fig. 8.7 are plotted from Eqs. (7.31) and (7.32) for the variations of the angles φ_{max} and φ_{min}, which are the upper and lower bonds of beam steering and pointing by Risley prism pairs in the B-1 and A-2 configurations, and beam steering and pointing are not possible in the pointing dead zone where $\varphi < \varphi_{min}$. The maximum deviation angle φ_{max} is one

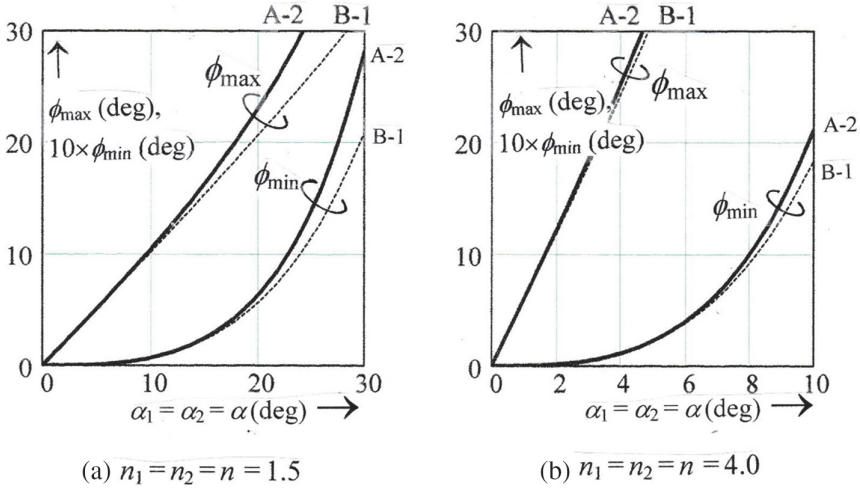

Figure 8.7 Computed results to show the dividing line of the pointing dead zone where $\varphi < \varphi_{min}$, and illustration and comparison of the numerical range of the extreme values of the deviation angles φ_{max} and φ_{min} of the rays emergent from the Risley prism pair beam steering systems in B-1 and A-2 configurations using two identical components of (a) vertex angle α from 0 to 30° and refractive index $n = 1.5$ and (b) α from 0 to 10° and refractive index $n = 4.0$.

order of magnitude larger than the minimum deviation angle $\varphi_{\min}$ and the curves shown the variations of $\varphi_{\min}$ in Fig. 8.7 are after $10\times$ scaling.

We have seen from the above discussion that the Risley prism pairs in four different configurations can be divided into two groups:

- The mirror symmetric group includes the Risley prism pairs in A-1 and B-2 configurations, for which no pointing dead zone, because the minimum ray deviation angle $\varphi_{\min} = 0$ and therefore they are applicable to laser beam pointing to targets within the circular cone around the axis of the system and with the half-apex angle $\varphi_{\max}$, that is the maximum angle of ray deviation.
- The B-1 and A-2 configurations are the asymmetric Risley prism pairs and there will be a small area in the paraxial region, to where the prisms can not point and is known as the blind zone of pointing, which will be discussed in greater detail in Chapter 9.

8.4 Generalization of the Inverse Solution from Precise Target Pointing to Highlight a Specific Pattern

Risley-prism-based beam-steering systems can be utilized to steer a laser beam to highlight a desirable pattern. This functionality is known as the synthesis of the scan pattern [6.1, 8.6, 8.7], which is a process opposite to scan pattern analysis, i.e., the inverse problem of finding the scan patterns produced by well-defined scanning systems. In this section, scan pattern synthesis utilizing Risley prism pairs is considered as a generalization of the exact solution of the inverse problem, which now extends from steering a laser beam to point at a point to steering a laser beam to highlight a specific pattern for laser lighting display or for creating desirable pattern for searching or tacking particular-shaped target. [8.12, 8.13]

8.4.1 Control law of Risley prism pairs for steering a laser beam to highlight a specific pattern

Assume the desirable pattern is described by the parametrization

$$x = x(\tau) \quad \text{and} \quad y = y(\tau), \tag{8.29}$$

where τ is a time-dependent parameter. Equation (8.21) in polar coordinates (ρ, φ) is given by

$$\rho(\tau) = \sqrt{x^2(\tau) + y^2(\tau)} \quad \text{and} \quad \varphi(\tau) = \arctan\frac{y(\tau)}{x(\tau)}. \tag{8.30}$$

Similar to Eq. (8.19) in Subsection 8.3.2, the Cartesian coordinates $[x(\tau), y(\tau)]$ for the scan pattern, as viewed from the far field region, can be expressed in terms of the direction cosines of the ray emergent from the system, given by

$$\frac{x(\tau)}{k_{2A}} = \frac{y(\tau)}{l_{2A}} = \frac{-P}{m_{2A}}, \tag{8.31}$$

where P is the distance from the prism pair to the plane of observation (see Fig. 8.1). Upon substituting from Eq. (5.3) into Eq. (5.2) and then making using $k_A^2 + l_A^2 + m_A^2 = 1$, we arrive at

$$\frac{\rho^2(\tau)}{P^2} = \frac{x^2(\tau) + y^2(\tau)}{P^2} = \frac{k_{2A}^2 + l_{2A}^2}{m_{2A}^2} = \frac{k_{2A}^2 + l_{2A}^2}{1 - (k_{2A}^2 + l_{2A}^2)}. \tag{8.32}$$

Again, after substituting from Eqs. (T7.3.1), (T7.3.3), and (T7.3.5) in Table 7.3 into Eq. (7.31) for k_A and l_A and then into Eq. (8.32), we obtain, after some rearranging, the expression

$$a_1^2 + a_3^2 \sin^2\alpha_2 + 2a_1 a_2 \sin\alpha_2 \cos(\Delta\theta) = \frac{\rho^2(\tau)}{P^2 + \rho^2(\tau)}, \tag{8.33}$$

where $\Delta\theta = \theta_2 - \theta_1$ represents the difference of prisms' orientations and $\Delta\theta$ or, the rotation angle of the second prism Π_2 relative to that of the first prism Π_1, that is, in general, a variable depending on the time-dependent parameter τ.

Comparing the structures of the expressions listed in Table 7.3 reveals that a_1 and a_2 are independent from $\Delta\theta$, but a_3 is a function of cos $\Delta\theta$, and their functional relationship can be expressed as

$$\cos(\Delta\theta) = \frac{1}{a_1 \sin\alpha_2}\left(\frac{1 - n_2^2 - a_3^2}{2a_3} + a_2 \cos\alpha_2\right). \tag{8.34}$$

After substituting from Eq. (8.34) into Eq. (8.33), we obtain the following second-order equation:

$$Aa_3^2 + Ba_3 + C = 0, \tag{8.35}$$

for which the solution is given by the quadratic formula

$$a_3 = \frac{-B \pm \sqrt{B^2 - 4AC}}{2A}, \tag{8.36}$$

where $A = \cos^2\alpha_2$, $B = -2a_2 \cos \alpha 2$, and

$$C = -a_1^2 - 1 + n_2^2 + \frac{\rho^2(\tau)}{P^2 + \rho^2(\tau)}.$$

Again, after substituting from a_3 in Eq. (8.36) into Eq. (8.34), we obtain

$$\Delta\theta = \arccos\left[\frac{1}{a_1 \sin\alpha_2}\left(\frac{1 - n_2^2 - a_3^2}{2a_3} + a_2 \cos\alpha_2\right)\right]. \tag{8.37}$$

To determine the rotation angles $\theta_1(\tau)$ and $\theta_2(\tau)$ for the two prisms, we return to Eqs. (8.30) and (8.31) and then re-express the expression for the angular coordinate ϕ in Eq. (8.30) in the form

$$\tan\phi(\tau) = \frac{y(\tau)}{x(\tau)} = \frac{l_A}{k_A} = \frac{a_1 \sin\theta_1 + a_3 \sin\alpha_2 \sin\theta_2}{a_1 \cos\theta_1 + a_3 \sin\alpha_2 \cos\theta_2}. \tag{8.38}$$

Due to $\Delta\theta = \theta_2 - \theta_1$, Eq. (8.38) can be rearranged in the form

$$\tan\phi(\tau) = \frac{a_1 \sin\theta_1 + a_3 \sin\alpha_2 \sin(\theta_1 + \Delta\theta)}{a_1 \cos\theta_1 + a_3 \sin\alpha_2 \cos(\theta_1 + \Delta\theta)} = \frac{\sin(\theta_1 + \theta_{10})}{\cos(\theta_1 + \theta_{10})} = \tan(\theta_1 + \theta_{10}). \tag{8.39}$$

where

$$\theta_{10} = \arctan\left(\frac{a_3 \sin\alpha_2 \sin\Delta\theta}{a_1 + a_3 \sin\alpha_2 \cos\Delta\theta}\right). \tag{8.40}$$

Now, we have enough parameters to express the rotation angles $\theta_1 = \theta_1(\tau)$ and $\theta_2 = \theta_2(\tau)$ of the two prisms in the form

$$\theta_1 = \phi(\tau) - \theta_{10} \quad \text{and} \quad \theta_2 = \phi(\tau) - \theta_{10} + \Delta\theta. \tag{8.41}$$

The pattern to be highlighted can be plotted out if we substitute Eq. (8.33) into Eq. (7.31) and then into Eqs. (8.23) and (8.22). However, you may find that one half of the desirable pattern can be plotted and another half is missing; this is because of the squaring effect introduced in the development of Eq. (8.24). This issue will be discussed in Part *A* in Subsection 8.3.2.

The usefulness of the above formulism will be shown by case studies regarding the creation of some fundamental patterns by Risley-prism-based beam steering system.

8.4.2 Straight line segment, circular and elliptical scan patterns produced by the Risley-prism-based beam-steering systems

A. A line segment produced by the Risley prism pair

Consider the creation of a straight line segment [see Fig. 8.8(a)] on the plane of observation located at a distance P from the Risley prism pairs system using two identical prisms of $n_1 = n_2 = n = 1.5$ and $\alpha_1 = \alpha_2 = \alpha = 5°$. The pattern to be created can be expressed parametrically in the form

$$x = x_m \cos\tau \quad \text{and} \quad y = 0, \tag{8.42}$$

where x_{m} is the half-length of the line segment along the x axis and the time-dependent parameter τ running from 0 to 2π.

After substituting from Eq, (8.35) into Eq. (8.22), we obtain

$$\rho(\tau) = x(\tau) = x_m \quad \text{and} \quad \phi(\tau) = 0. \tag{8.43}$$

Solution of the quadratic formula in Eq. (8.28) for the coefficient a_3 can be expressed more explicitly as

$$a_3 = \frac{a_2\sqrt{1 + (\rho(\tau)/P)^2} \pm 1}{\cos\alpha_2\sqrt{1 + (\rho(\tau)/P)^2}}. \tag{8.44}$$

Equation (8.37) is the discriminant of selecting the plus and minus signs in Eq. (8.44) if a real number solution for $\Delta\theta$ can be obtained from that equation.

Using Eqs. (8.36) and (8.41), we are able to plot $\Delta\theta$, θ_1 and θ_2 against the time-dependent parameter τ in Figs. 8.8(b) and 8.8(c) under the condition of $x_{\mathrm{m}} = 0.2P$. From Fig. 8.8(b), we found the two extreme values $(\Delta\theta)_1 = 86.9°$ and $(\Delta\theta)_2 = 180°$ in the variation of the relative rotation angle $\Delta\theta$ against the time-dependent parameter τ.

Figure 8.8(c) is plotted from Eq. (8.41) to show the rotation angles θ_1 and θ_2 of the two prisms, which reveal the pendulum-like oscillatory rotation of the two prisms for a line segment generation.

Between the two curves, there is a gap of $\Delta\theta = \theta_2 - \theta_1$ that changes periodically with the time-dependent parameter τ, and it attains the minimum value of $(\Delta\theta)_1 = 86.9°$ when $\tau = 0$, π and $2\pi \ldots$, and the maximum value of $(\Delta\theta)_2 = 180°$ when $\tau = 0.5\pi$ and $1.5\pi \ldots$, i.e., when the power of ray deviation by the system attains minima, because $(\Delta\theta)_2 = 180°$ implies the apexes of the two prisms oppose.

Numerical results reveal the potential of generation of a line segment longer than $x_{\mathrm{m}} = 0.2P$ if the relative rotation angles $(\Delta\theta)_1$, $(\Delta\theta)_2]$ of the two prisms changes from [86.9°, 180°] to [0°, 180°] to increase scan line length from $0.22P$ to the maximum scan line length of $0.2862P$ as predicted by Eq. (8.29) for system using two identical prisms of refractive index $n = 1.5$ and apex angle $\alpha = 15°$, and for an infrared system of $n = 4.0$ and $\alpha = 5°$ the maximum scan line length is $0.6368P$.

Finally, it is worth of noting

- Only the line segment from $x = 0$ to $+x_{\mathrm{m}}$ can be plotted from Eq. (8.41) because of the squaring effect introduced in the development of Eq. (8.32). The another half $x = -x_{\mathrm{m}}$ to 0 is plotted from $-\sqrt{x^2}$.

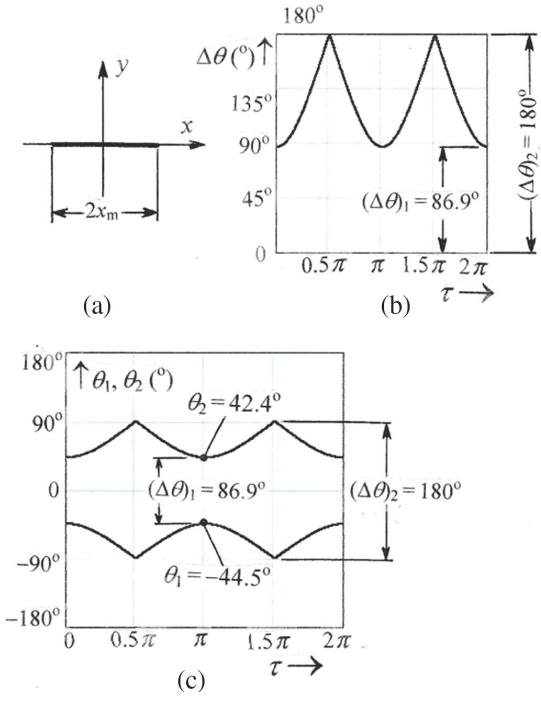

Figure 8.8 Synthesis of a straight line segment by Risley prism pair in the A-1 configuration and using two identical prisms of refractive index $n = 1.5$ and opening angle $\alpha = 5°$. (a) Illustration of the straight line segment of $x_m = 0.2P$ in length to be created along the x axis. (b) The relative rotation angle between the two prisms as a function of the time-dependent parameter τ and (c) The motion curves of the two prisms showing their rotation angles θ_1 and θ_2 as functions of τ.

- The evidence to support the correctness of the formulism and discussion presented above is the direction cosine $l_A \equiv 0$ [see Eq. (7.32)] for any value of the time-dependent parameter τ.

B. A circular pattern produced by the Risley prism pair

Consider the creation of a circular pattern [see Fig. 8.9(a)] on the plane of observation located at a distance P from the Risley prism pairs system using two identical prisms of $n_1 = n_2 = n = 1.5$ and $\alpha_1 = \alpha_2 = \alpha = 5°$. The pattern to be created can be expressed parametrically in the form

$$x = r_0 \cos\tau \quad \text{and} \quad y = r_0 \sin\tau, \tag{8.45}$$

where r_0 is radius of the circle and the time-dependent parameter τ running from 0 to 2π.

Making use of the Eqs. (8.36) and (8.41), we are able to plot $\Delta\theta$, θ_1 and θ_2 against the time-dependent parameter τ in Figs. 8.9(b) and 8.9(c) under the condition of $r_0 = 0.2P$.

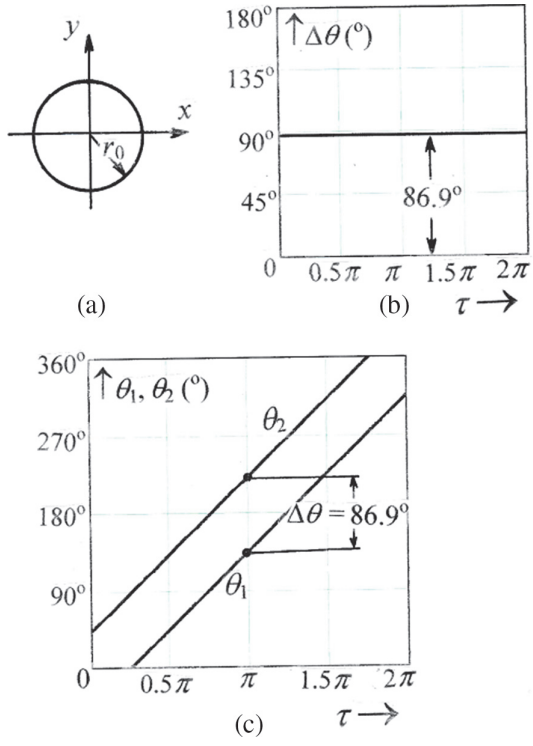

Figure 8.9 Creation of a circular pattern by Risley prism pair in the A-1 configuration and using two identical prisms of refractive index $n = 1.5$ and opening angle $\alpha = 5°$. (a) The circular pattern of radius $r_0 = 0.2P$ and centered on the axis of the system to be created on the plane of observation at distance P. (b) The relative rotation angle $\Delta\theta$ between the two prisms as a function of the time-dependent parameter τ. (c) Motion curves of the two prisms showing their rotation angles θ_1 and θ_2 as functions of τ.

From Fig. 8.9(b), we found the relative rotation angle $\Delta\theta = \theta_2 - \theta_1 = 86.9°$ is not a variable that implies the two prisms with different orientation will be rotated as a whole to create the circular pattern. As a result of $\Delta\theta =$ constant, Fig. 8.9(c) shows two parallel lines on the two sides of a gap of 86.9°. Similar to the creation of the line scan of the maximum length $0.2862P$, the maximum radius of circle is $0.2862P$ that can be created by system using two identical prisms in parallel and characterized by refractive index $n = 1.5$ and apex angle $\alpha = 15°$; and for an infrared system of $n = 4.0$ and $\alpha = 5°$, the maximum radius is $0.6368P$.

C. An elliptical pattern produced by the Risley prism pair

Consider the creation of an elliptical pattern [see Fig. 8.10(a)] on the plane of observation located at a distance P from the Risley prism pairs system using two identical prisms of $n_1 = n_2 = n = 1.5$ and $\alpha_1 = \alpha_2 = \alpha = 5°$. The pattern to be created can be expressed parametrically in the form 7.25, 8.8]

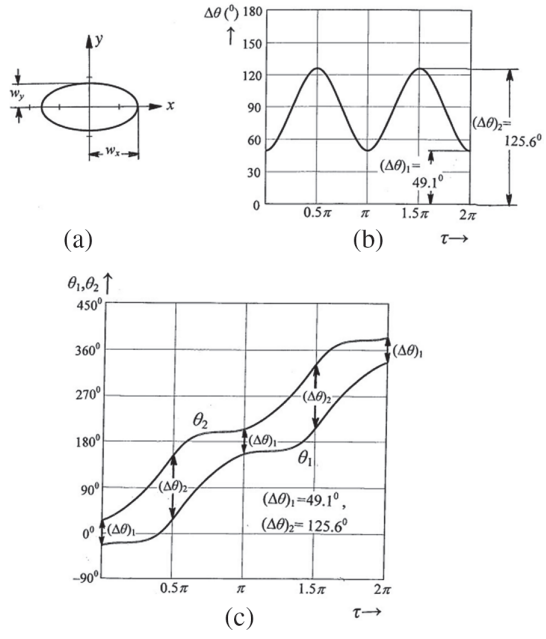

Figure 8.10 Synthesis of an elliptical pattern by Risley prism pairs in the A-1 configuration and using two identical prisms of refractive index $n = 1.5$ and opening angle $\alpha = 5°$. (a) The elliptical pattern to be created, (b) The relative rotation angle of the two prisms as a function of the time-dependent parameter τ and (c) Motion curves of the two prisms showing their rotation angles θ_1 and θ_2 as functions of τ.

$$x = w_x \cos\tau \quad \text{and} \quad y = w_y \sin\tau, \tag{8.46}$$

where w_x and w_y are the major and minor axes coinciding with the x and y axes and the time-dependent parameter τ running from 0 to 2π.

Under the condition of $w_x = 0.08P$ and $w_y = 0.04P$, the angle $\Delta\theta$ showing relative rotation between the prisms Π_2 and Π_1 is plotted from Eq. (8.37) and displayed in Fig. 8.10(b), from the curve we found the two extreme values $(\Delta\theta)_1 = 49.1°$ and $(\Delta\theta)_2 = 129.6°$ in the variation of $\Delta\theta$ when the time-dependent parameter τ runs from 0 to 2π.

The two curves in Fig. 8.10(c) are plotted from Eq. (8.41) to show the dependence of prism rotation angles θ_1 and θ_2 on the time-dependent parameter τ. The two curves are not equally spaced, the change of spacing with the parameter τ showing the variations of $\Delta\theta$ that attains the minimum value of $(\Delta\theta)_1 = 49.1°$ when $\tau = 0$, π and 2π ... when the power of the two prism combination attains the peak value of ray deviation for the requirement of generating the major axis of the ellipse. After this point, the power of the two prism combination decreases to minimum value of $(\Delta\theta)_2 = 129.6°$ when $\tau = 0.5\pi$ and 1.5π....

Correctness of the above discussion can be checked by using the computed results shown on Fig. 8.10(c). For example, when $\tau = 0$ laser spot is at the point ($x = w_x$, $y = 0$), Fig. 8.10(c) shows the orientations of the prisms Π_1 and Π_2 are at $\theta_1 = -\ (\Delta\theta)_1/2 = -24.6°$ and $\theta_2 = +(\Delta\theta)_1/2 = 24.6°$, respectively. At this point, the power of ray deviation by the prisms Π_1 and Π_2 combination is proportional to $2[\cos(\Delta\theta)_1/2]$, as shown by Eq. (7.6). Similarly, at the point of ($x = 0$, $y = w_y$) we have $\theta_1 = 90° - (\Delta\theta)_2/2$ and $\theta_1 = 90° + (\Delta\theta)_2/2$ where $(\Delta\theta)_2 = 125.6°$, the resultant deviation is proportional to 2 $[\cos(\Delta\theta)_2/2]$. The ratio of the two resultant deviations is given by

$$[\cos(\Delta\theta)_1/2]/[\cos(\Delta\theta)_2/2] = [\cos(49.2°/2)]/[\cos(125.6^o)/2] = (0.9092/0.4571) = 1.989,$$

which is close enough to the ratio of major/minor axis of the elliptical scan pattern, i.e., $\varepsilon = w_x/w_y = 2$.

8.5 Exact Analytic Solutions of Two-Element Risley Prism Pointers

We have so far considered a closed-form analytical solution for the inverse problem of Risley prism pointers in different configurations (see, Fig. 7.7). Results obtained in Section 8.3.1 have been considered exact due to the use of the vector-based Snell's law for non-paraxial ray tracing of a ray through a pair of wedges without relying on the approximate technique such as $\sin x \cong x - x^3/6$ that implies no particular quantitative limitation on the selection of their opening angles, however, that was considered as a good approximation to the case of pointing targets at a large distance away from the pointer, because of the ignorance of the thickness of the two prisms and the width of the air gap between them. The aim of this Section is twofold

1) To show the exactness of the theories presented in Section 8.3.1 in predicting correct results for pointing and tracking targets traversing both he near- and far-regions of the field in front of the pointer if the linear size of the targets greater than a small fraction of the central thickness of the prism;

2) To provide an analytic solution for tracking targets of any size in both the near- and far-regions of the field in front of the pointer.

Figure 8.11(a) shows the ray path in a Risley prism pair with refractive surfaces 11 and 12 of the first prism Π_1 and 21 and 22 of the second prism Π_2, the distances between the centers of the four refractive surfaces are d_1, d_{air} and d_2, and the points of ray-and-interface intersection are shown by the position vectors $\mathbf{r}_{11}$, $\mathbf{r}_{12}$, $\mathbf{r}_{21}$, $\mathbf{r}_{22}$, respectively, or by the position vectors $\boldsymbol{\rho}_{11}$, $\boldsymbol{\rho}_{12}$, $\boldsymbol{\rho}_{21}$, $\boldsymbol{\rho}_{22}$ which are obtained by projecting the three-dimensional $\mathbf{r}$-vectors onto the plane of $z = 0$. Determination of $\mathbf{r}_{22}$ or $\boldsymbol{\rho}_{22}$ is the starting point to find the

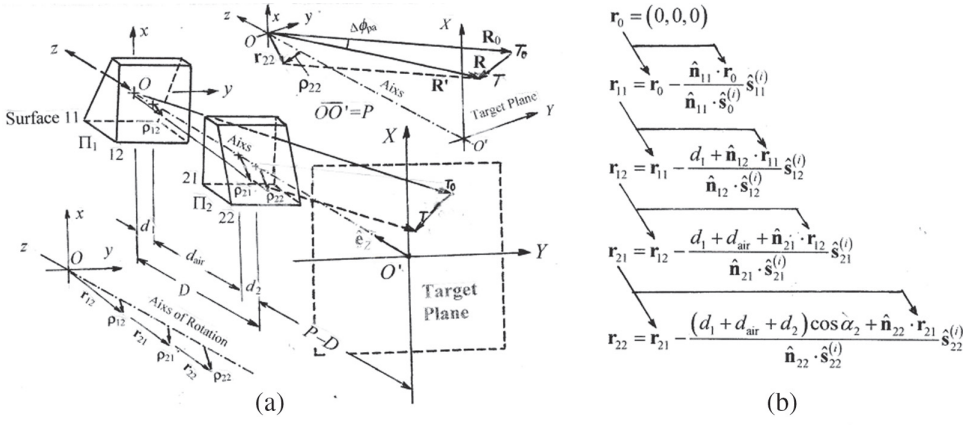

Figure 8.11 (a) Schematic diagram showing the distribution of the intersection points of ray and prism surfaces in the two-element Risley prism poining system. Definition of position vectors ($\mathbf{r}_{11}$, $\mathbf{r}_{12}$, $\mathbf{r}_{21}$, $\mathbf{r}_{22}$) of the intersection points and their projections ($\boldsymbol{\rho}_{11}$, $\boldsymbol{\rho}_{12}$, $\boldsymbol{\rho}_{21}$, $\boldsymbol{\rho}_{22}$) on the plane $z = 0$ (see the insert on lower left). Target $\boldsymbol{T}_0$ and its pointing vector $\mathbf{R}_0$ and the angular difference $\Delta\phi_{\text{pa}}$ between pointing vectors $\mathbf{R}_0$ and $\mathbf{R}$ after taking the prism thickness and air gap into account (see the insert on upper right). (b) Illustrating the recursion relations to find the distribution of ray-surfaces intersection points in Risley prism pointer.

exact inverse solution of Risley prism pointers because the far field solution described in Section 8.2.1 was grown up under the assumption of $d = d_{\text{air}} = d_2 = 0$ that is equivalent to assume $\mathbf{r}_{22}$ and $\boldsymbol{\rho}_{22} = 0$, which may provide exact results under certain conditions.

8.5.1 Locus of the point where the ray exits the pointer and the validity of the solution presented in section 8.3.1

Using the expressions listed in Table 7.1 relating to the ray refractions at the interfaces 11, 12,..., 22 inside a Risley prism pointer, and then we may use Eq. (1.9) to find the ray-and-interface intersection points one-by-one from the point $\mathbf{r}_{11}$ to the point of $\mathbf{r}_{22}$ through a recurring operation, shown by the flow chart in Fig. 8.11(b). Specifically, the recurring operation starts from the poit $\mathbf{r}_{11} = (0,0,0)$, i.e., the point of incidence to the pointer. After substituting from $\mathbf{r}_{11}$ into the equation in the second row of Fig. 8.11(b), we obtain the point of $\mathbf{r}_{12}$ on the second surface 12 of the first prism, from which we find point $\mathbf{r}_{21}$ on the other side of the air gap, i.e., on the first surface 21 of the second prism and finally we obtain the position vector of point $\mathbf{r}_{22}$ that can be expressed as

$$\mathbf{r}_{22} = \frac{d_1}{\hat{\mathbf{n}}_{12} \cdot \hat{\mathbf{s}}_{12}^{(i)}} \mathbf{D}_1 + \frac{d_1 + d_{\text{air}}}{\hat{\mathbf{n}}_{21} \cdot \hat{\mathbf{s}}_{21}^{(i)}} \mathbf{D}_2 + \frac{(d_1 + d_{\text{air}} + d_2)\cos\alpha_2}{\hat{\mathbf{n}}_{22} \cdot \hat{\mathbf{s}}_{22}^{(i)}} \mathbf{D}_3 \tag{8.47}$$

with

$$\mathbf{D}_1 = -\hat{\mathbf{s}}_{12}^{(i)} + \frac{\hat{\mathbf{n}}_{21}\cdot\hat{\mathbf{s}}_{12}^{(i)}}{\hat{\mathbf{n}}_{21}\cdot\hat{\mathbf{s}}_{21}^{(i)}}\hat{\mathbf{s}}_{21}^{(i)} + \frac{\hat{\mathbf{n}}_{22}\cdot\hat{\mathbf{s}}_{12}^{(i)}}{\hat{\mathbf{n}}_{22}\cdot\hat{\mathbf{s}}_{22}^{(i)}}\frac{\hat{\mathbf{n}}_{21}\cdot(\hat{\mathbf{s}}_{21}^{(i)} - \hat{\mathbf{s}}_{12}^{(i)})}{\hat{\mathbf{n}}_{21}\cdot\hat{\mathbf{s}}_{21}^{(i)}}\hat{\mathbf{s}}_{22}^{(i)},$$
$$\mathbf{D}_2 = -\hat{\mathbf{s}}_{21}^{(i)} + \frac{\hat{\mathbf{n}}_{22}\cdot\hat{\mathbf{s}}_{21}^{(i)}}{\hat{\mathbf{n}}_{22}\cdot\hat{\mathbf{s}}_{22}^{(i)}}\hat{\mathbf{s}}_{22}^{(i)} \quad \text{and} \quad \mathbf{D}_3 = -\hat{\mathbf{s}}_{22}^{(i)}.$$

After a tedious but straightforward algebra, we obtain from Eq. (8.47) the position vector for the point where the ray (or the axis of the beam) exits the pointer in the form

$$\begin{aligned}\mathbf{r}_{22} = (x_{22},\, y_{22},\, z_{22}) &= \mathbf{r}_{\mathrm{o}} - \frac{D\cos\alpha_2 + \hat{\mathbf{n}}_{22}\cdot\mathbf{r}_{\mathrm{o}}}{\hat{\mathbf{n}}_{22}\cdot\hat{\mathbf{s}}_{22}^{(i)}}\hat{\mathbf{s}}_{22}^{(i)} \\ &= (0,\, 0,\, \Delta z_3) - (D + \Delta z_3)\cos\alpha_2\frac{(a_1\cos\theta_1,\, a_1\sin\theta_1,\, a_2)}{F_{\mathrm{A}}(\Delta\theta)},\end{aligned} \tag{8.48}$$

in which $\mathbf{r}_{\mathrm{o}} = (0,\, 0,\, \Delta z_3)$ and $D = d_1 + d_{\mathrm{air}} + d_2$, $\Delta z_3 = d_{\mathrm{air}}\left(\sqrt{(n_1^2 - a_1^2)/(1 - a_1^2)} - 1\right)$ is the conic point of Corn #3 in Fig. 7.2(a) and the parameters a_1, a_2 and the function $F_{\mathrm{A}}(\Delta\theta)$ can be found in Table 7.3.

To show the quantitative data of the influence of $D \neq 0$ on pointing accuracy, let us consider the vector $\boldsymbol{\rho}_{22}$ that is the projection of the position vector $\mathbf{r}_{22}$ onto the plane of $z = 0$. The magnitude of $\boldsymbol{\rho}_{22}$ represents the off-axis distance of the point where the ray exits the pointer. Using $(k_{2\mathrm{A}}^{(i)},\, l_{2\mathrm{A}}^{(i)},\, m_{2\mathrm{A}}^{(i)})$ in Eq. (7.23) to replace $\hat{\mathbf{s}}_{22}^{(i)}$, we obtain from Eq. (8.48) that

$$|\boldsymbol{\rho}_{22}| = \sqrt{x_{22}^2 + y_{22}^2} = \frac{(D + \Delta z_3)|a_1|\cos\alpha_2}{|F_{\mathrm{A}}(\Delta\theta)|}, \tag{8.49}$$

which is plotted in Fig. 8.12 for systems using matched pairs of wedge prisms of refractive index $n = 1.5$ and $d_1 = d_2 = d$ with $d_{\mathrm{air}}/d = 1$, 0.5 and 0.1 as a parameter. We obtain $|\boldsymbol{\rho}_{22}|/d = 0.102$ when the wedge angle $\alpha = 5°$ and $d_{\mathrm{air}}/d = 1$, and $|\boldsymbol{\rho}_{22}|/d = 0.205 \sim 0.207$ when the wedge angle $\alpha = 10°$ and $d_{\mathrm{air}}/d = 1$. it is also seen that off-axis distance reduces with decreasing values of d_{air}/d.

Figure 8.12 reveals for edge angle $\alpha_1 = \alpha_2 \leq 10°$ the off-axis distance is as small as a fraction of the central thickness d of the prisms, if we combine this outcome with the fact that the targets in the real-world are not geometric points, but material objects of certain size. This situation encourages us for a rational consideration of the consequence of ignoring the thickness of prisms and the air gap separation and then giving a criterion to define the region in

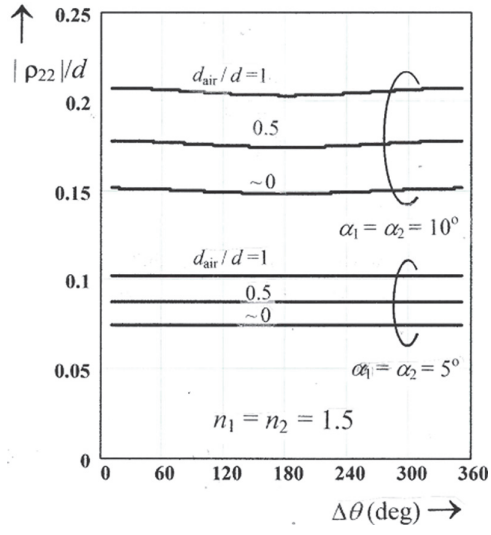

Figure 8.12 Off-axis distance plotted from Eq. (8.49) for the magnitude of the vector $\boldsymbol{\rho}_{22}$ normalized by prisms central thickness. $\boldsymbol{\rho}_{22}$ is the projection of the position vector $\mathbf{r}_{22}$ onto the plane of $z = 0$, and $\mathbf{r}_{22}$ is the position vector of thee point where the ray exists the pointer.

front of the pointer, in which the noniterative analytic solutions shown in subsection 8.3.1 predict correct results about detecting and tracking targets of different size. To do this, let us return to Section 7.3 and have a close look at Eqs. (7.31) and (7.32) and their related parameters listed in Tables 7.3 and 7.4 and then one may readily find that the ray direction vector $\hat{\mathbf{s}}_{22}^{(r)}$ for the ray exiting the pointer is independent from (d_1, d_2; d_{air}) but is determined by the characterization parameters (n_1, n_2; α_1, α_2) and the orientations (θ_1, θ_2) of the prisms. This is understandable because the refraction of rays at the interfaces of the prisms inside a Risley prism pair is at points in planar surfaces between two medium of constant refractive indexes and with constant surface normal to all points within the clear apertures of the prisms. Consequently, the Snell's law yields the same degree of deviation for all the rays at the same angle of incidence to any points within the clear apertures of the prisms regardless to the thickness and the air gap separation between them. We may therefore conclude that the prisms thickness related parameters (d_1, d_2 ; d_{air}) have no effect on the direction of the beam steered by the pointer, they effect mainly on the location of the point, specified by the position vector $\mathbf{r}_{22}$, on the interface 22, where the beam leaves the device, as illustrated in Fig. 8.11(a). This finding helps us to understand the validity of the solutions presented in subsection 8.3.1, which may predict correct results for targets traversing across both the near- and far-regions of the filed in front of the pointer under certain conditions. Moreover, this finding is not limited by two-element Risley prism pointer, it can be generalized to systems of more than two elements and

also to the case when the ray of incidence is not coincided with the axis of rotation.

Using the invariance property of the ray direction vector $\hat{\mathbf{s}}_{22}^{(r)}$, we may readily graph the ray path diagram for a traditional Risley prism pointer in Figs. 8.11 and 8.13 in which the unit vector $\hat{\mathbf{s}}_{220}^{(r)}$ [see Eq. (8.51b) below] is shown between two vectors $\mathbf{R}_0$ and $\mathbf{R}'$ to stress they are parallel and in the same direction. Specifically, $\mathbf{R}_0$ is the target position vector predicted by the solutions presented in the subsection 8.3.1 when the target is assumed in the direction specified by the altitude Φ and azimuth Θ, however, this vector starts from the origin O of the coordinates and ended at the point T_0 that is a point in the surface of the target. On the other hand, the vector $\mathbf{R}'$ is the ray-path vector representing the ray actually departing from the pointer, which starts from the tip of the position vector $\mathbf{r}_{22}$ on the interface 22 and ended at the point T on the same plane for the target. Apparently, T_0 and T are two points in the target plane, between them there is a separation $\left|\overrightarrow{T_0T}\right|$ as shown in Fig. 8.13, which represents the pointing inaccuracy caused by the ignorance of the influence of prism thickness related parameter. Since the computed results of $|\overrightarrow{T_0T}|$ plotted in Fig. 8.14 reveal that $\left|\overrightarrow{T_0T}\right|$ is a small fraction of prism thickness and, therefore, it may simply be filled up by the linear size $L_{\min}$ of the target, or by the radius $R_{\min}$ of the beam radius or by their combination, in which the last possibility is shown in Fig. 8.13 and can be expressed as

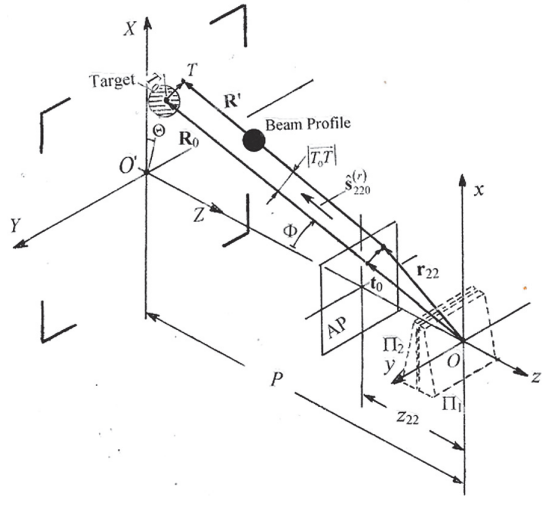

Figure 8.13 Ray path diagram for a graphic analysis of the pointing inaccuracy caused by the separation $|\overrightarrow{T_0T}|$ between the target position vector $\mathbf{R}_0$ and the ray-path vector $\mathbf{R}'$. Illustrating the methods for filling up the separation by the targets with sufficiently large linear size, by beam radius or by their combination.

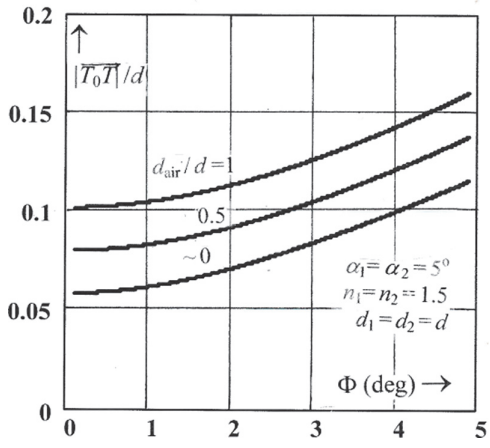

Figure 8.14 Plot of Eq. (4.6) to show the pointing inaccuracy by the ignorance of prisms thickness and the air gap between them. The separation $|\overrightarrow{T_0T}|$ between the two points T_0 and T, i.e., the endpoints of the target position vector and the outgoing ray direction vector is the graphic equivalent term of the pointing inaccuracy.

$$L_{\min} + R_{\min} > |\overrightarrow{T_0T}|. \tag{8.50}$$

The next step is an evaluation of $|\overrightarrow{T_0T}|$ based on the following expression of the target that is located at a distance P away from the origin O and in the direction specified by (Φ, Θ):

$$\mathbf{R}_0 = (\cos\Theta\tan\Phi,\ \sin\Theta\tan\Phi,\ -1)P, \tag{8.51a}$$

where a positive P (> 0) is assumed and the unit vector of $\mathbf{R}_0$, given by

$$\hat{\mathbf{s}}_{220}^{(r)} = \left(k_{22}^{(r)},\ l_{22}^{(r)},\ m_{22}^{(r)}\right) = \mathbf{R}_0/|\mathbf{R}_0| = (\cos\Theta\sin\Phi,\ \sin\Theta\sin\Phi,\ -\cos\Phi) \tag{8.51b}$$

After setting up an auxiliary plane (AP) at $z = z_{22}$ in Fig 8.13, we find the width of the separation $|\overrightarrow{T_0T}|$, given by

$$|\overrightarrow{T_0T}| = |\mathbf{r}_{22} - \mathbf{t}_0| = \left|\mathbf{r}_{22} + \frac{z_{22}}{\cos\Phi}\hat{\mathbf{s}}_{220}^{(r)}\right| \tag{8.52a}$$

where the vector $\mathbf{t}_0$ is a portion of the target position vector $\mathbf{R}_0$, that starts at the origin O and ended at a point in the AP. After substituting from $\mathbf{r}_{22}$ in Eq. (8.48) and $\hat{\mathbf{s}}_{22}^{(r)}$ in Eq. (8.51b) into Eq. (8.52a), we have

$$|\overrightarrow{T_0T}| = \sqrt{(x_{22} + z_{22}\cos\Theta\tan\Phi)^2 + (y_{22} + z_{22}\sin\Theta\tan\Phi)^2}, \tag{8.52b}$$

which is plotted in Fig. 8.14 and it is seen that $|\overrightarrow{T_0T}|$ is small, usually $(0.05 \sim 0.15)d$.

As an example, let us consider a matched pair of wedge prisms of $\alpha_1 = \alpha_2 = 5°$, $n_1 = n_2 = 1.5$ and prism central thickness $d_1 = d_2 = 10$ mm, and then we obtain from Fig. 8.14 that under the condition of the linear size of the target $L_{\min} > 1.5$ mm or the radius of the laser beam $R_{\min} > 1.5$ mm, the solutions presented in subsection 8.3.1 can be used to predict correct results for detecting and tracking targets in both the near- and far-regions of the bear-steering field produced by the Risley prism pointer when used for a wide variety of applications.

It is also interesting of noting that Fig. 8.14 shows the decreasing values of $|\overrightarrow{T_0T}|$ with decreasing width of the air gap, which implies that we may reduce the air gap as far as possible to increase the distinguishing ability of the pointer.

8.5.2 Exact solutions of two-element Risley prism pointers for tracking targets of any size

Both the forward and inverse solutions are obtained from solving the equation of the beam steering field under different conditions. For example, we may obtain from Eq. (7.15) an expression for beam steering field produced by the traditional Risley prism pointer when $\mathbf{r}_{22} = 0$ in the form

$$\mathbf{R} = -\frac{P}{m_{2A}}\hat{\mathbf{s}}_{2A}, \tag{8.53a}$$

where the direction vector $\hat{\mathbf{s}}_{2A} = (k_{2A}, l_{2A}, m_{2A})$ of the ray departing the pointer can be found from Eq. (7.31). The forward solution of Eq. (8.53a) is a mathematical statement for R when the direction vector $\hat{\mathbf{s}}_{2A}$ is known, whereas the inverse solution is a statement of $\hat{\mathbf{s}}_{2A}$ when the target position vector $\mathbf{R}$ is known. For example, the target direction vector is known as $\mathbf{R} = (\cos\Theta\tan\Phi,\ \sin\Theta\tan\Phi,\ -1)P$, then we may obtain from Eq. (8.53a) the key equations for the inverse problem in the forms

$$\cos\Theta\tan\Phi = k_{2A}/m_{2A},\ \sin\Theta\tan\Phi = l_{2A}/m_{2A} \tag{8.53b}$$

and then

$$m_{2A} = -\cos\Phi \text{ or, } k_{2A}^2 + l_{2A}^2 = \sin^2\Phi \quad \text{and} \quad \tan\Theta = \frac{l_{2A}}{k_{2A}} \tag{8.53c}$$

which are shown in Eqs. (8.11a), (G2b) in the Appendix G and (8.13a), respectively.

For the case of $\mathbf{r}_{22} = 0$, we obtain from Eq. (7.15) a similar, but more elaborate, expression in the form

$$\mathbf{R} = \mathbf{r}_{22} - \frac{P + z_{22}m_{2A}}{m_{2A}}\hat{\mathbf{s}}_{2A} = (x_{22},\, y_{22},\, z_{22}) - \frac{P + z_{22}m_{2A}}{m_{2A}}\hat{\mathbf{s}}_{2A}, \tag{8.54a}$$

in which $\mathbf{r}_{22}$ and its components can be found in Eq. (8.48). Similar to Eq. (8.53b) derived from Eq. (8.53a), we may find the following expressions from Eq. (8.54a):

$$\left\{\cos\Theta\tan\Phi = (x_{22}/P) - \frac{1 + (z_{22}/P)}{m_{2A}}k_{2A}, \right. \tag{8.54b}$$

$$\left\{\sin\Theta\tan\Phi = (y_{22}/P) - \frac{1 + (z_{22}/P)}{m_{2A}}l_{2A}. \right. \tag{8.54c}$$

The square sum of the above two equations yields

$$\frac{x_{22}^2 + y_{22}^2}{P^2} - 2\frac{x_{22}k_{2A} + y_{22}l_{2A}}{P}\frac{1 + (z_{22}/P)}{m_{2A}} + \left(1 + \frac{z_{22}}{P}\right)^2\frac{k_{2A}^2 + l_{2A}^2}{m_{2A}^2} = \tan^2\Phi, \tag{8.54d}$$

in which we find that the three terms on the left hand are functions of $\cos\Delta\theta$, i.e.,

$$\left.\begin{aligned} x_{22}^2 + y_{22}^2 &= \frac{(D + \Delta z_3)^2 a_1^2\cos^2\alpha_2}{F_A^2(\cos\Delta\theta)}, \\ x_{22}k_{2A} + y_{22}l_{2A} &= -\frac{(D + \Delta z_3)a_1\cos\alpha_2}{F_A(\cos\Delta\theta)}[a_1 + a_3(\cos\Delta\theta)\sin\alpha_2\cos\Delta\theta], \\ \frac{k_{2A}^2 + l_{2A}^2}{m_{2A}^2} &= \frac{1}{[a_2 - a_3(\cos\Delta\theta)\cos\alpha_2]^2} - 1. \end{aligned}\right\} \tag{8.54e}$$

After substituting from Eq. (8.54e) into Eq. (8.54d) we find a sextic polynomial in one element $\cos(\Delta\theta)$, which reduces to Eqs. (8.11a) or to (G2b) in the Appendix G when

$$P \gg D.$$

Using the root-finding algorithm, the zero points of the polynomial in Eq. (8.54d) are obtained and listed in Table 8.3 for systems using matched Risley prism pairs of refractive index $n = 1.5$ and wedge angle $\alpha = 5°$ for the purpose of tracking a target in the direction of ($\Phi = 4.5°$, $\Theta = 120°$) and located at a distance P from the origin O of coordinates system sited at the center of the first surface of the prism Π_1, for which the central thickness and the air gap between Π_1 and Π_2 are assumed identical, i.e., $d_1 = d_{air} = d_2 = d$.

Table 8.3 Computed results of Eq. (8.54d) showing the relative rotation angle $\Delta\theta$ and the orientations (θ_1, θ_2) of the two prisms in the Risley prism pointer for tracking a target in the direction of altitude $\Phi = 4.5°$ and azimuth $\Theta = 120°$ and at different distance P normalized by prism central thickness d. Assume the pointer in the A-1 configuration using matched pair of index $n = 1.5$, wedge angle $\alpha = 5°$and identical central thickness of the prisms and the air gap between them.

P/*d*	$\Delta\theta$	θ_1	θ_2	Related Equations
$\to \infty$	52.939°	93.443°	146.383°	(8.11a) and (8.13a)
10^5	52.936°	93.444°	146.380°	
10^4	52.901°	93.462°	146.363°	(8.54d) and (8.54e)
10^3	52.556°	93.635°	146.191°	
10^2	48.922°	95.459°	144.381°	
20	25.157°	107.382°	132.539°	

The computed results listed in the Table 8.3 are the relative rotation angle $\Delta\theta$, the orientations (θ_1, θ_2) of the two prisms and the normalized target distance P/d, running from 20, 10^2, 10^3,... to 10^5, i.e., in the range from 20 (cm) to 1 (km) when $d = 1$cm. The data on the table show a reduction of the values of $\Delta\theta$ with decreasing values of target distance. This relationship is comprehensible because the altitude Φ of the target is defined by the LOS from the central point O of the first surface of the prism Π_1 to the target, whereas the altitude (say, Φ') of the ray (i.e., the axis of the laser beam) pointing to the same target is defined from the ray-exiting point near the center of the second surface of the prism Π_2, since the ray-exiting point is closer to the target than the point O does, so we have $\Phi' > \Phi$ and it is worth noting that the difference between Φ' and Φ increases continuously as the target moving in the direction to the pointer, which implies there is a continuous demand to bring down the relative rotation angle $\Delta\theta$ of the two prisms to meet with the requirement of increasing the ray deviation angle that is supposed to be obtained from the Risley prism pointer, however, the pointer fails to meet this expectation when the target moves to the point of $P = 15.8d$ where the altitude Φ' of the ray pointing to the target reaches its upper limit, given by $\varphi_{\max} = 5.032139°$ [see, e.g., Eq. (8.15)] that is the maximum angle of ray deviation by the matched pair of $n = 1.5$ and $\alpha = 5°$, where $\Phi' = \varphi_{\max}$ the relative rotation angle of the two prisms $\Delta\theta = 0$. After the point of $P = 15.8d$, the pointer is still able to work normally for target tracking if its altitude Φ reduces to a level below 4.5°. For example, it may be used for tracking a target of $\Phi = 3.0°$ until the target moves to the point $P = 4.2d$ in the immediate neighborhood in front of the pointer.

The main results of this section may be summarized by a comparison of the merits and limitations of theory presented in the subsection 8.3.1 [see, e.g., Eqs. (8.11a) and (8.13a)] with the predictions of Eq. (8.54d). Both of them are exact inverse solutions because they are able to predict correct results in both the near- and far-regions, however,

- Equations (8.11a) and (8.13a) are closed-form analytic solutions and applicable for tracking targets traversing the immediate neighborhood in front of the pointer if their linear size is greater than a small fraction of the central thickness of the prism.
- No limitation on the size of the targets is the exceptional merit of Eq. (8.54d) that may therefore be used as the control law of the pointer for high accuracy pointing and tracking tiny targets if they are not traversing the immediate neighborhood in front of the pointer because the tracking process may suddenly be interrupted by the critical point determined by the condition of $\Phi' = \varphi_{\max}$, aside from this unfavorable issue is the search of the zero point of the sixtic polynomial shown in Eq. (8.54d), which may take more computer time than that for solving the simple equations shown in (8.11a) and (8.13a) that can compute the solution to the same problem in a finite number of steps and be used as the initial guess for the zero point searching.

Finally it is worthy to mention that the Risley prism pointer is a nonlinear device and has to face the control singularity problems. To fix them, limited zones are placed around the singularities to assure a controllable motion of the two prisms at the price of a reduction of the relative rotation angle $\Delta\theta$ and the maximum angle of ray deviation $\varphi_{\max}$, which implies a reduction of the tracking range. For improvement a third prism can be added to eliminate some of the unfavorable issues as shown in the next chapter.

Bibliography and Links

[8.1] C. T. Amirault and C. A. DiMarzio, "Precision pointing using a dual-wedge scanner," *Appl. Opt.* **24**, 1302–1308(1985).

[8.2] G. C. Boisset, B. Robertson, and H. S. Hinton, "Design and construction of an active alignment demonstrator for a free-space optical interconnect," *IEEE Photon. Technol. Lett.* **7**, 676–678 (1995).

[8.3] J. J. Degnan," Ray matrix approach for the real time control of SLR2000 optical elements," in 14th International Workshop on Laser Ranging (2004).

[8.4] Y. Yang, "Analytic solution of free space optical beam steering using Risley prism pair," *J. Lightwave Technol.,* . **26**, 3576–3583 (2008).

[8.5] M. Born and E. Wolf, *Principles of Optics*, *7th ed.* (Cambridge U. Press, 1999), Sec. 3.2.2.

[8.6] G. Garcia-Torales, M. Strojnik, and G. Paez, "Risley prism pair to control wave-front tilt and displacement in a vectorial interferometer," *Appl. Opt.*, **41**, 1380–1384 (2002).

[8.7] W. C. WargerII and C. A. DiMarzio, "Dual-wedge scanning confocal reflectance microscope," *Opt. Lett.*, **32**, 2140–2142 (2007).

[8.8] Y. Li, "Closed form analytical inverse solutions for Risley-prism based beam steering systems in different configurations," *Appl. Opt.* **50**, 4302–4309 (2011).

[8.9] R. Paschotta, "Noise in Laser Technology– Part 3: Beam Pointing Fluctuations," *Laser Technik Journal 7 (1)*, **48** (2010). RUL: https://www.rp-photonics.com/article_noise_in_laser_technology3.html

[8.10] URL: https://www.rp-photonics.com/beam_pointing_fluctuations.html

[8.11] Wikipidia: Log-log Plot.. URL: https://en.wikipedia.org/wiki/log_log_plot

[8.12] A. Li, X. Liu, and W. Sun, "Forward and inverse solutions for three-element Risley prism beam scanners," *Opt. Express*, **25**, 7677–7688 (2017). URL: https://www.osapublishing.org/oe/ abstract.cfm?uri=oe-25-7-7677

[8.13] A. Li, X. Gao, W. Sun, W. Yi, Y. Bian, H. Liu, and L. Liu, "Inverse solutions for a Risley prism scanner with iterative refinement by a forward solution," *Appl. Opt.*, **54**, 9981–9989 (2015).